



# Advanced MRI Protocols to Discriminate Glioma From Treatment Effects: State of the Art and Future Directions

Dania G. Malik<sup>1</sup>, Tanya J. Rath<sup>1</sup>, Javier C. Urcuyo Acevedo<sup>2</sup>, Peter D. Canoll<sup>3</sup>, Kristin R. Swanson<sup>2</sup>, Jerrold L. Boxerman<sup>4</sup>, C. Chad Quarles<sup>5</sup>, Kathleen M. Schmainda<sup>6</sup>, Terry C. Burns<sup>7</sup> and Leland S. Hu<sup>1,2\*</sup>

<sup>1</sup> Department of Radiology, Mayo Clinic, Phoenix, AZ, United States, <sup>2</sup> Mathematical Neurooncology Lab, Precision Neurotherapeutics Innovation Program, Mayo Clinic, Phoenix, AZ, United States, <sup>3</sup> Departments of Pathology and Cell Biology, Columbia University, New York, NY, United States, <sup>4</sup> Department of Diagnostic Imaging, Brown University, Providence, RI, United States, <sup>5</sup> Department of Neuroimaging Research & Barrow Neuroimaging Innovation Center, Barrow Neurologic Institute, Phoenix, AZ, United States, <sup>6</sup> Department of Biophysics & Radiology, Medical College of Wisconsin, Milwaukee, WI, United States, <sup>7</sup> Departments of Neurologic Surgery and Neuroscience, Mayo Clinic, Rochester, MN, United States

## OPEN ACCESS

### Edited by:

Nicoletta Anzalone,  
San Raffaele Hospital (IRCCS), Italy

### Reviewed by:

Virginia Hill,  
Northwestern University, United States  
Emanuele Pravata,  
Ente Ospedaliero Cantonale  
(EOC), Switzerland

### \*Correspondence:

Leland S. Hu  
Hu.Leland@mayo.edu

### Specialty section:

This article was submitted to  
Neuroradiology,  
a section of the journal  
Frontiers in Radiology

Received: 04 November 2021

Accepted: 01 March 2022

Published: 15 April 2022

### Citation:

Malik DG, Rath TJ, Urcuyo  
Acevedo JC, Canoll PD, Swanson KR,  
Boxerman JL, Quarles CC,  
Schmainda KM, Burns TC and Hu LS  
(2022) Advanced MRI Protocols to  
Discriminate Glioma From Treatment  
Effects: State of the Art and Future  
Directions. *Front. Radiol.* 2:809373.  
doi: 10.3389/fradi.2022.809373

In the follow-up treatment of high-grade gliomas (HGGs), differentiating true tumor progression from treatment-related effects, such as pseudoprogression and radiation necrosis, presents an ongoing clinical challenge. Conventional MRI with and without intravenous contrast serves as the clinical benchmark for the posttreatment surveillance imaging of HGG. However, many advanced imaging techniques have shown promise in helping better delineate the findings in indeterminate scenarios, as posttreatment effects can often mimic true tumor progression on conventional imaging. These challenges are further confounded by the histologic admixture that can commonly occur between tumor growth and treatment-related effects within the posttreatment bed. This review discusses the current practices in the surveillance imaging of HGG and the role of advanced imaging techniques, including perfusion MRI and metabolic MRI.

**Keywords:** post-treatment, glioblastoma, MRI, response assessment, advanced, perfusion, metabolic

## INTRODUCTION

Treatment of high-grade gliomas (HGGs) requires a multidisciplinary approach, with the standard of care first-line treatment comprising the combination of maximal safe surgical cytoreduction, followed by adjuvant radiotherapy and chemotherapy (1). Posttreatment surveillance imaging plays a vital role in assessing the therapeutic response and disease progression/recurrence to guide the clinical management and tailored therapy for each patient. Contrast-enhanced MRI (CE-MRI), with and without intravenous administration of a gadolinium-based contrast agent (GBCA), is considered to be the clinical benchmark for imaging follow-up (2). However, the use of CE-MRI alone can be limited in distinguishing the overlapping features of tumor progression and posttreatment-related effects. Specifically, both entities can present as contrast-enhancing lesions due to blood-brain-barrier (BBB) disruption with resultant vasogenic edema. Both entities can also progress over time and present as serially enlarging masses on follow-up imaging (3).

Multiple advanced imaging techniques including perfusion and metabolic MRI provide additional biomarkers of tissue characteristics that can improve the diagnostic specificity. Perfusion techniques include dynamic susceptibility contrast (DSC) MRI based on T2- or T2\*-weighted susceptibility effects of intravascular contrast agent, to measure microvasculature features

including microvessel volume. Dynamic contrast enhanced (DCE) MRI, another perfusion technique, can measure features such as vascular leakage based on T1-weighted (T1W) relaxivity effects related to BBB permeability, while arterial spin labeling (ASL) uses the magnetic labeling of arterial blood as an endogenous contrast agent to primarily measure blood flow. The use of perfusion MRI techniques relies on the premise that HGG recurrence will exhibit higher vascularity (microvessel volume, blood flow) compared to non-tumoral posttreatment effects. Magnetic resonance spectroscopy (MRS) is a form of metabolic imaging that can quantify specific metabolites (e.g., choline, lipid/lactate, and glutamine/glutamate) associated with tumor growth, necrosis, and posttreatment effects.

These techniques have been widely applied in the setting of posttreatment HGG, as evidenced by the myriad of published studies in this field of research. These techniques are also widely available in clinical practice, which speaks to their immediate clinical translation and impact. However, there are persisting obstacles to widespread adoption, including discrepancies and variability in the published thresholds/criteria for diagnosis and the perceived utility of each technique. These issues are multifactorial, but technical factors and the integrity of validation methods are likely contributors, particularly in the setting of intratumoral heterogeneity and histologic admixture. In this review, we critically assess the literature to date and discuss some of the contributing factors to this variability, including the differences in image acquisition, protocol design, and validation methods. We highlight the methodologies promoting consistency, accuracy, and robustness of advanced perfusion and metabolic imaging for HGG- response assessment. We also discuss the need for spatially resolved validation methods to overcome the challenges of intratumoral heterogeneity. Finally, we summarize the recent efforts in the development of consensus recommendations for the acquisition of perfusion MRI in HGG and discuss the needs moving forward for clinical implementation and widespread adoption.

## CURRENT TREATMENT PRACTICES

The current treatment of HGG consists of maximal safe surgical resection followed by adjuvant radiotherapy and chemotherapy. Radiotherapy has been used since the 1970s after survival benefit was seen with its use following surgical resection of HGGs (4). The Stupp protocol (5), published in 2005, showed that the addition of temozolomide (TMZ), a cytotoxic alkylating agent, to adjuvant radiotherapy further contributed to survival benefit. The Stupp protocol is currently the standard of care for glioblastoma (GBM) and consists of 6 weeks of concomitant adjuvant radiotherapy and chemotherapy with TMZ followed by 6 months of TMZ alone. Additional FDA-approved therapies include other cytotoxic alkylating agents (lomustine, intravenous carmustine, and carmustine wafer implants), bevacizumab, a vascular endothelial growth factor (VEGF) inhibitor, and an electric field therapy referred to as Tumor Treating Fields. Systemic administration of alternate alkylating agents is less well tolerated than the TMZ and is usually reserved for tumor

recurrence (6). There are different reports regarding the effect of bevacizumab on overall survival (7), but it does decrease vasogenic edema and can temporarily improve the quality of life for inoperable recurrent disease resistant to standard therapies. However, the phenomenon of “pseudoresponse” has been well reported after bevacizumab therapy, in which the imaging signs of decreased BBB permeability (and vessel leakage) are not reflective of a true decrease in the tumor burden (8). Despite standard multi-modal therapy, the median survival of patients with HGG remains poor, particularly in the setting of isocitrate dehydrogenase (IDH) wild-type tumors. In the case of GBM, the most aggressive form of HGG which comprises nearly 50% of all gliomas, the median survival is approximately 15 months (5). These poor outcomes have motivated the efforts to identify novel therapeutic strategies, including targeted small molecule therapies, metabolically-targeted therapies, and immunotherapies, in attempts to improve the treatment response and overall survival.

Many emerging passive and active immunotherapy treatments for HGG are currently being evaluated in clinical trials, attempting to combat the immunosuppressive characteristics of glioma to bolster the treatment efficacy (9, 10). The HGGs have been shown to elicit severe reductions in the number and function of CD4 T lymphocytes (11). This can be reversed with the blockade of inhibitory pathways leading to increased T-cell response and activation, and subsequently increased the antitumor activity of these immune cells. Mouse models have demonstrated improved survival with the use of anti-programmed cell death protein (anti-PD-1) immune checkpoint inhibitors for intracranial glioma (12), and nivolumab and pembrolizumab, both anti-PD-1 agents, have been evaluated in multiple recent and ongoing clinical trials. Cytotoxic T-lymphocyte-associated protein 4 (CTLA-4), lymphocyte activation gene 3 (Lag3), and indoleamine 2,3-dioxygenase (IDO) are additional immune checkpoint inhibitors that affect the T- lymphocyte activation pathway, and they have induced tumor regression and improved the long-term survival in murine glioma models, particularly when used in combination (11).

Active immunotherapy regimens capable of inducing antitumor response include multiple vaccine-based treatments. Dendritic cell-based vaccines, already FDA-approved for prostate cancer treatment, also increased survival in preclinical GBM models (13). Dendritic cells are a type of antigen-presenting cell derived from a patient's CD14+ monocytes, loaded with tumor antigens *in vitro*, and subsequently injected back into the patient to activate T-cell and B-cell responses (14). Peptide vaccines are comprised of synthetic amino acid chains mimicking proteins that are over-expressed by tumors. Current peptide vaccines under investigation target the isocitrate dehydrogenase 1 (IDH1), epidermal growth factor receptor variant III (EGFRvIII), and human leukocyte antigens (HLAs) (10). Oncolytic viruses, already FDA-approved for metastatic melanoma, are recombinant viruses, such as adenovirus or herpes simplex virus (HSV) that are used to infect and destroy tumor cells. The safety, efficacy, and long-term effects of oncolytic viruses in glioma treatment are currently

under investigation (9). Chimeric antigen receptor (CAR)-T cell therapy utilizes CARs that are bound to a patient's T-cells (15). The CAR-T cell therapy is FDA-approved for hematologic malignancies (9), showing robust efficacy in preclinical models and has demonstrated a proof of principle in refractory human GBM (16). Despite a strong biological premise and promise in the early phase trials, showing evidence of biological efficacy based upon early radiographic evidence of pseudoprogression, no immunotherapy regimen has yet demonstrated improved survival in a randomized phase 3 trial for GBM. These translational challenges increase the urgency to improve individual longitudinal analysis of individual human gliomas through improved radiographic analyses.

## TREATMENT-RELATED EFFECTS

Posttreatment radiation effects (PTREs), which include pseudoprogression and radiation necrosis, have been well documented following chemoradiation, with a similar phenomenon following immunotherapy (17, 18), and can confound the assessment of treatment response both clinically and on imaging findings. A spectrum of imaging findings and histologic changes in the treated tumor field can be presented with or without associated clinical symptoms. Pseudoprogression has been defined as treatment effects immediately after or soon after radiotherapy leading to perceived tumor progression on the follow-up imaging and subsequent improvement without any change in the intervention (17). Pseudoprogression is generally used to describe early PTRE occurring within 3–6 months after the initiation of adjuvant therapy (19), while radiation necrosis typically occurs beyond 6 months of completing the therapy, but can occur early, mid, or late (even after many years) after the completion of adjuvant therapy (20). Both entities are believed to be manifestations of radiation-induced effects, and both were documented in postradiotherapy patients prior to the widespread use of TMZ (21). However, the added effect of TMZ appears to increase the incidence of pseudoprogression and radiation necrosis (22, 23), presumably due to increased radiosensitization by the cytotoxic agent (19, 24). Pseudoprogression has been associated with improved overall survival in multiple studies (25, 26), and it has been suggested that the presence of pseudoprogression could correlate with the efficacy of therapy (27). The presence of radiation necrosis has also been associated with the improved rate of survival, although some studies suggest that this association may be influenced by the timing of radiation necrosis development and confirmation on biopsy. One study reported improved survival when radiation necrosis was diagnosed from biopsies obtained more than 5 months after treatment (28). Another study suggests that radiation necrosis is associated with improved progression-free survival as well as the overall survival from the time of recurrence, rather than from the initial diagnosis (29).

The pathophysiology of PTRE is not completely understood but is suggested to be a combination of inflammation, edema, myelin destruction, and changes in the vessel permeability resulting in the breakdown of BBB (30). These findings may

be transient in the setting of pseudoprogression but do not always resolve spontaneously with radiation necrosis. Pathologic specimens of pseudoprogression changes have been described as bland necrosis, vascular fibrinoid necrosis, reactive gliosis, demyelination, and vascular hyalinization (31) and there is considerable overlap with the pathologic changes seen with radiation necrosis. The incidence of pseudoprogression has a wide variation across studies, but a meta-analysis of 73 studies demonstrated a pooled incidence of 36% after standard therapy for HGG with a range of 0–64% (32). A greater incidence of pseudoprogression has been shown in gliomas with methylated MGMT promoter status compared to the unmethylated status (27). The reported incidence of radiation necrosis ranges from 3 to 24% (3). Clinical symptoms can accompany the development of PTRE and include headache, nausea, or dizziness that are related to increased intracranial pressure. These symptoms are typically managed with steroid therapy unless the patient is taking immune checkpoint inhibitor therapy, in which case, symptoms are managed with bevacizumab, as steroids counteract the therapeutic effects of immune checkpoint inhibitors. In some cases, additional treatments are required, including bevacizumab, Laser Interstitial Thermal Therapy, or surgical resection (33).

Immunotherapy for gliomas and other cancers is well documented to increase the incidence of pseudoprogression (34, 35). The mechanism is not fully elucidated but is presumably related to the direct inflammatory response caused by the activation of the immune system (36). Reports of histologic changes specific to glioma are lacking, but the histology of pseudoprogression seen in the melanoma of brain metastases demonstrated clusters of tumor cells with surrounding reactive astrocytosis, inflammatory cells, and microglial cells (37). Generalized neuroradiologic changes and neurotoxicities, such as aseptic encephalitis or meningitis, have also been documented in the use of immunotherapy for tumors outside of the CNS (38–40), and these changes could contribute to the posttreatment effects of immunotherapy for HGG.

## CURRENT USE OF POSTTREATMENT IMAGING FOLLOW-UP

Contrast-enhanced MRI is considered the golden standard for the follow-up of brain tumors, and the protocols are largely based on the standardized brain tumor imaging protocol (BTIP) consensus recommendations published in 2015 (2). The minimum standard protocol includes 3D pre- and postcontrast T1-weighted sequences, axial 2D T2-weighted sequence, axial 2D FLAIR, and axial 2D diffusion-weighted imaging (DWI). Following surgical resection, baseline postoperative imaging is usually acquired within 24–48 h to evaluate the degree of tumor removal, which has important prognostic implications (41), and to provide a baseline for subsequent imaging. The National Comprehensive Cancer Network (NCCN) guidelines recommend an initial follow-up imaging of 2–8 weeks later following the completion of adjuvant therapy (1). Subsequent imaging will be spaced out every 2–4 months for 3 years and then every 3–6 months indefinitely.

Traditionally, response assessment was determined on the basis of measurable enhancement using the Macdonald Criteria (42). The 2010 Response assessment in neuro-oncology (RANO) criteria have since superseded the Macdonald Criteria and account for other imaging characteristics that may be present in addition to or instead of an enhancement (43). In particular, the RANO criteria acknowledge that gliomas may demonstrate T2/FLAIR changes only without enhancement. Therefore, the RANO criteria define tumor progression as “greater than or equal to 25% increase in the sum of the products of perpendicular diameters of enhancing lesions measurable enhancement” or “significant progression in T2/FLAIR changes” (43). These criteria also take into account the changes in steroids and symptoms to help compensate for the limitations of interpreting imaging without clinical context (44). Due to the prevalence of pseudoprogression within the first 3 months of initiating therapy, the RANO criteria recommend defining progression within the first 3 months only if it is confirmed pathologically or if the majority of enhancement is outside the radiation field. Given the multiple emerging immunotherapy options for brain tumors, the immunotherapy RANO (iRANO) criteria were later published in 2015 and further expand on the recommendations related to pseudoprogression (36). In patients with the early imaging signs of progression, within 6 months of initiating immunotherapy, iRANO advocates for confirmatory imaging no sooner than 3 months after the initial radiologic progression. Despite the development of these criteria, there are limitations described below that limit the practical application in the routine clinical use, due in large part to the non-specificity of contrast-enhancement (which could represent tumor or posttreatment effect) and histologic admixture within a single lesion.

## Limitations of Conventional CE-MRI and Challenges Due to Intratumoral Heterogeneity

The overlapping imaging characteristics of PTRE and tumor progression on CE-MRI are well recognized (17, 19, 36, 43). Both tumor and PTRE can present as enlarging, enhancing masses with the surrounding vasogenic edema on serial conventional CE-MRI examinations. These imaging features relate to the extravasation of contrast into the tissues secondary to vascular leakage and BBB disruption (45). The non-enhancing edema seen on T2/FLAIR imaging is presumably related to increased water content from associated vascular leakage. However, this can be further complicated by the likely admixture of non-enhancing tumors that can infiltrate the peritumoral vasogenic edema regions surrounding the enhancing core (46).

Aside from the difficulties in distinguishing the appearance of tumor and PTRE on CE-MRI, histologic admixture commonly occurs, such that tumor growth can (and arguably typically does) occur within a background of treatment-related changes (46–49). This admixture can occur within a single biopsy specimen, as highlighted recently in a study by Winter et al. (50) from a large cohort of biopsy-proven cases of pseudoprogression and radiation necrosis. But at the same time, studies have also shown that foci of tumor recurrence can be spatially distinct

from the regions of pure PTRE within different regions of a single MRI-enhancing lesion, which suggests the different spatial scales of intralesional histologic heterogeneity (51, 52). While most studies on intralesional heterogeneity have been within the context of the posttreatment setting following standard chemo-radiation, intralesional heterogeneity is also well documented following immune therapies, with admixed regions of tumor growth co-occurring with the adjacent regions of pseudoprogression/posttreatment changes (36, 53). Importantly, this heterogeneity also increases the risk of surgical sampling errors, as the histologic diagnosis from one biopsy location may not accurately reflect the diagnosis from other regions of the same MRI enhancing lesion (46). Further, variability in the histologic admixture within individual biopsy specimens also opens the door to variability in histologic criteria to define HGG vs. PTRE. The clinical utility of quantifying relative tumor burden within an enhancing lesion is still being investigated, as some studies have shown that histologic tumor fraction (i.e., the proportion of residual tumor) has important prognostic implications (54), while others failed to show a significant correlation with the survival (55). However, to the extent that imaging may be relevant to interpret the therapeutic response to a presumed recurrent tumor, the ability to reliably discriminate tumor from treatment effects could help accelerate the therapeutic translation and help decrease the guesswork currently inherent to patient management.

## ADVANCED IMAGING TECHNIQUES AND PRINCIPLES

### Perfusion Imaging

Perfusion MRI comprises a variety of functional imaging techniques, supplemental to conventional MRI, that can provide additional information related to hemodynamics and vascularity of tissues. Perfusion techniques include dynamic susceptibility contrast (DSC), dynamic contrast enhanced (DCE), and arterial spin labeling (ASL) imaging. Both DCE and DSC require exogenous GBCA while ASL uses the endogenous contrast of magnetic labeling. Many studies have shown that perfusion MRI techniques, in general, can provide valuable additional information to standard MRI in the assessment of brain tumors, particularly when assessing the post-treatment effects of HGG.

Dynamic susceptibility contrast-based perfusion imaging is based on the paramagnetic susceptibility effects of GBCA on the acquired MRI signal. DSC is also termed “bolus-tracking” MRI, as the first pass of a contrast bolus through the brain tissue is dynamically evaluated with gradient echo (GRE) T2\*-weighted or spin echo (SE) T2-weighted images (56, 57). The intravascular and extravascular compartments experience differing susceptibility effects from GBCA and each contributes to the acquired signal. The voxel-wise change in signal over time can be mapped to a contrast concentration-time curve which can be further analyzed to create parametric maps of relative cerebral blood volume (rCBV) and relative cerebral blood flow (rCBF). Additional derived parameters include peak height (PH) and the

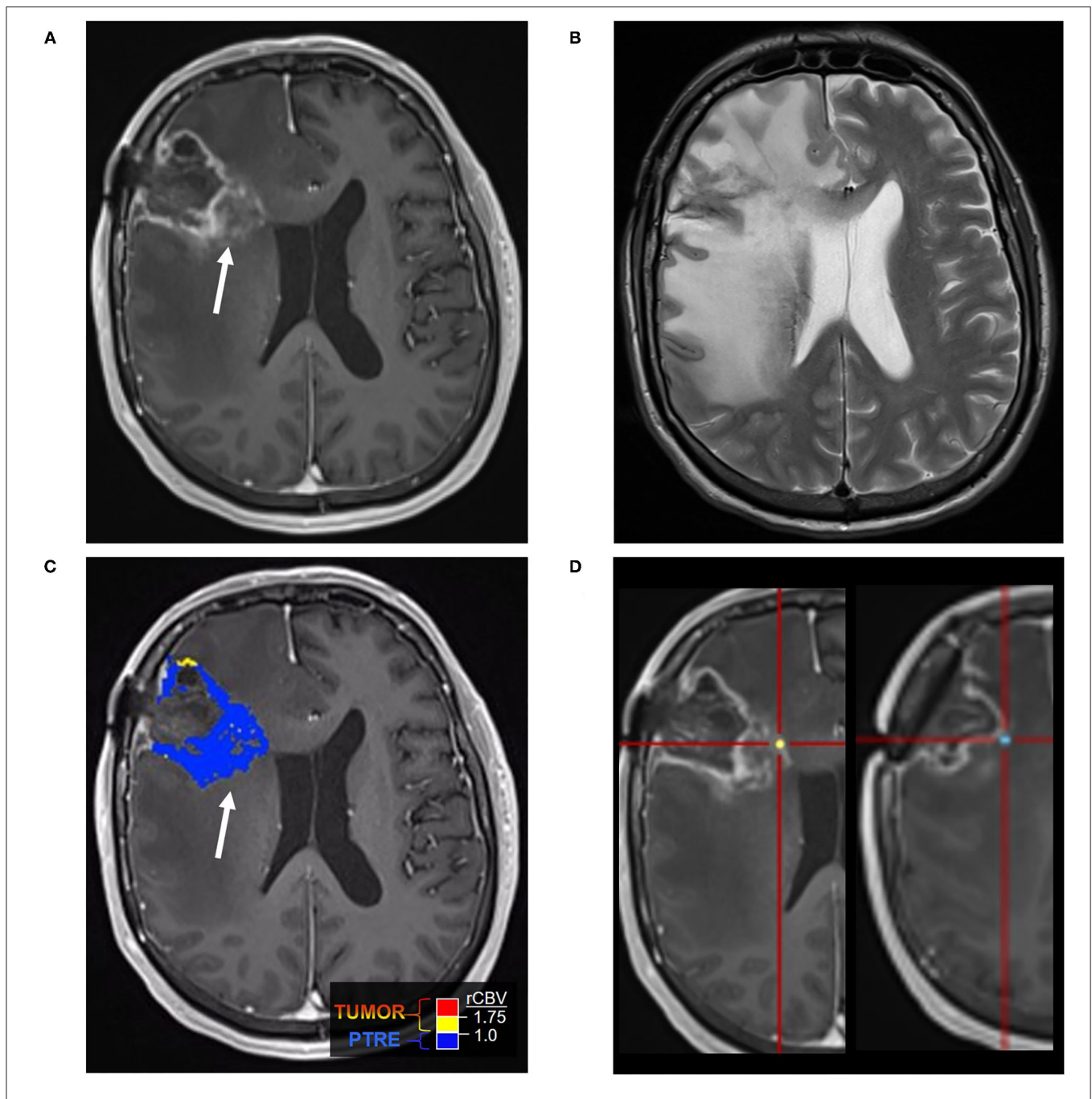
percentage of signal intensity recovery (PSR). PH is defined as the maximum signal intensity loss during bolus tracking compared to the baseline, and it has been shown to correlate with CBV (58). PSR is based on the signal recovery relative to baseline after the first pass of contrast bolus and is influenced by vessel permeability, acquisition parameters, as well as cell density and cell size (59).

Among these various advanced DSC-MRI metrics, rCBV represents the most commonly employed and widely published metric for distinguishing tumor recurrence from PTRE. This is based on the biological premise that vascular volume (and thus rCBV measurement) significantly differs between the two entities, as HGG recurrence exhibits higher microvessel volume compared to the PTRE (60, 61) (**Figures 1–3**). As such, tumor is associated with higher rCBV compared to PTRE. Given the quantitative nature of rCBV, and the clinical importance of distinguishing tumor from PTRE, there has been tremendous interest in identifying reliable rCBV thresholds to differentiate HGG from treatment effects (57, 62–67). A recent meta-analysis by Patel et al. (68) has highlighted many of these studies and reported 28 studies using DSC-MRI for evaluating gliomas after radiation and/or chemotherapy, a pooled accuracy of approximately 85% for mean rCBV. This body of literature, and the clinical accessibility of the DSC-MRI technique, have helped drive widespread clinical adoption of DSC-MRI for rCBV measurement to aid in the differential diagnosis of tumor vs. PTRE for HGG-response assessment. At the same time, this meta-analysis also highlighted the wide variability in the reported rCBV thresholds across different studies, which ranged from 0.9 to 2.15 for mean rCBV. This variability has likely led to confusion within the neuro-oncologic field regarding the reliability of the predictive diagnostic threshold criteria to distinguish tumors from PTRE. For example, one institution may recommend the rCBV threshold of 1.0 (above which would favor the diagnosis of tumor, and below which would favor the diagnosis of PTRE), while another institution may favor an rCBV threshold of 1.75. While several important factors contribute to this variability, addressing these issues will facilitate the development of universal diagnostic guidelines across institutions for incorporating rCBV thresholds in response assessment.

The first factor relates to the differences in the validation methods that compare rCBV with the histologic classification of tumor vs. PTRE. For example, in the first type of validation method, some studies lack surgical biopsy specimens and histologically confirmed diagnoses when classifying MRI enhancing lesions as tumor vs. PTRE (69, 70). While these studies instead rely on serial imaging, the non-specific nature of MRI, and the fact that PTRE can exactly mimic tumor as enlarging enhancing masses on MRI, may lead to the misclassification of tumor vs. PTRE, which can confound the reliability of the reported rCBV thresholds distinguishing the two entities. Furthermore, as discussed above, the spatial and histologic heterogeneity of tumor and PTRE can complicate the use of CE-MRI in tracking the temporal evolution of enhancing lesions, as the radiographic appearance of MRI enhancement and edema may be influenced by the relative abundance of tumor and PTRE. Meanwhile, the second type of validation

method is the use of non-localizing biopsies as a form of histologic confirmation to classify MRI enhancing lesions as tumor vs. PTRE (71). This generally involves the use of a biopsy specimen from an unspecified location within the MRI enhancing lesion to classify the entire lesion as either tumor or PTRE, based on histologic criteria. As the location of the biopsy (and thus the corresponding location for rCBV measurement) is undocumented, the rCBV value of a particular lesion is generally measured from the entire MRI enhancing volume. This creates a spatial discrepancy between the measured rCBV and the histologic diagnosis, which can be confounded by intratumoral heterogeneity (as detailed in the previous heading), which increases the risk of sampling errors in the diagnosis and histologic misclassification (**Figure 2**). Also, as MRI enhancing lesions invariably comprise a variable histologic admixture of tumor and PTRE components, the measured rCBV across the entire lesion is likely influenced by these admixed components. Finally, there are also differences in the histologic criteria across studies that are used to define tumor vs. PTRE classifications. For instance, one study required that surgical samples contain at least 20% of tumor components to classify an MRI enhancing lesion in the “tumor” category (64), while lower histologic thresholds (i.e., 0–20%) were used by other studies (49, 51, 52, 61, 72). All of these factors can not only influence the accuracy of the reported rCBV thresholds to distinguish tumor from PTRE but also likely contribute to the variability in the reported threshold values themselves, as published by one institution vs. another. The third type of validation method relates to the use of image-localized biopsies to record the stereotactic locations of surgical specimens that are submitted for histologic diagnosis, which are then spatially correlated with the localization of regional rCBV measurements from the corresponding biopsy locations. There are several distinct advantages to this method of histologic validation. This spatially accurate method of correlating the localized rCBV with individual biopsy samples addresses the confounds of histologic heterogeneity at the regional spatial scale, which can refine the rCBV thresholds distinguishing tumors from PTRE. Also, the use of individual biopsy specimens as separate “observations” within a large enhancing mass can improve the likelihood of isolating histologically “pure” PTRE vs. “pure” tumor (49, 52, 61), which addresses the histologic heterogeneity at the biopsy scale. Finally, the use of localized regional rCBV measurements (on the order of less than 10 voxels per region of interest) can facilitate the identification of rCBV thresholds that distinguish tumor vs. PTRE at the regional level, and even at the voxel level, which allows for the use of rCBV to differentiate and quantify the regions of tumor vs. PTRE within the admixed lesions (46, 49, 51, 52, 61, 73). Identifying regionally-specific tumor populations and the regions of PTRE can help overcome clinical sampling errors by guiding surgical biopsy targets that are specific to foci of tumor recurrence which not only aids clinical diagnostic confirmation of tumor progression but can also help isolate adequate tumor burden for other applications, such as molecular profiling and investigational assays.

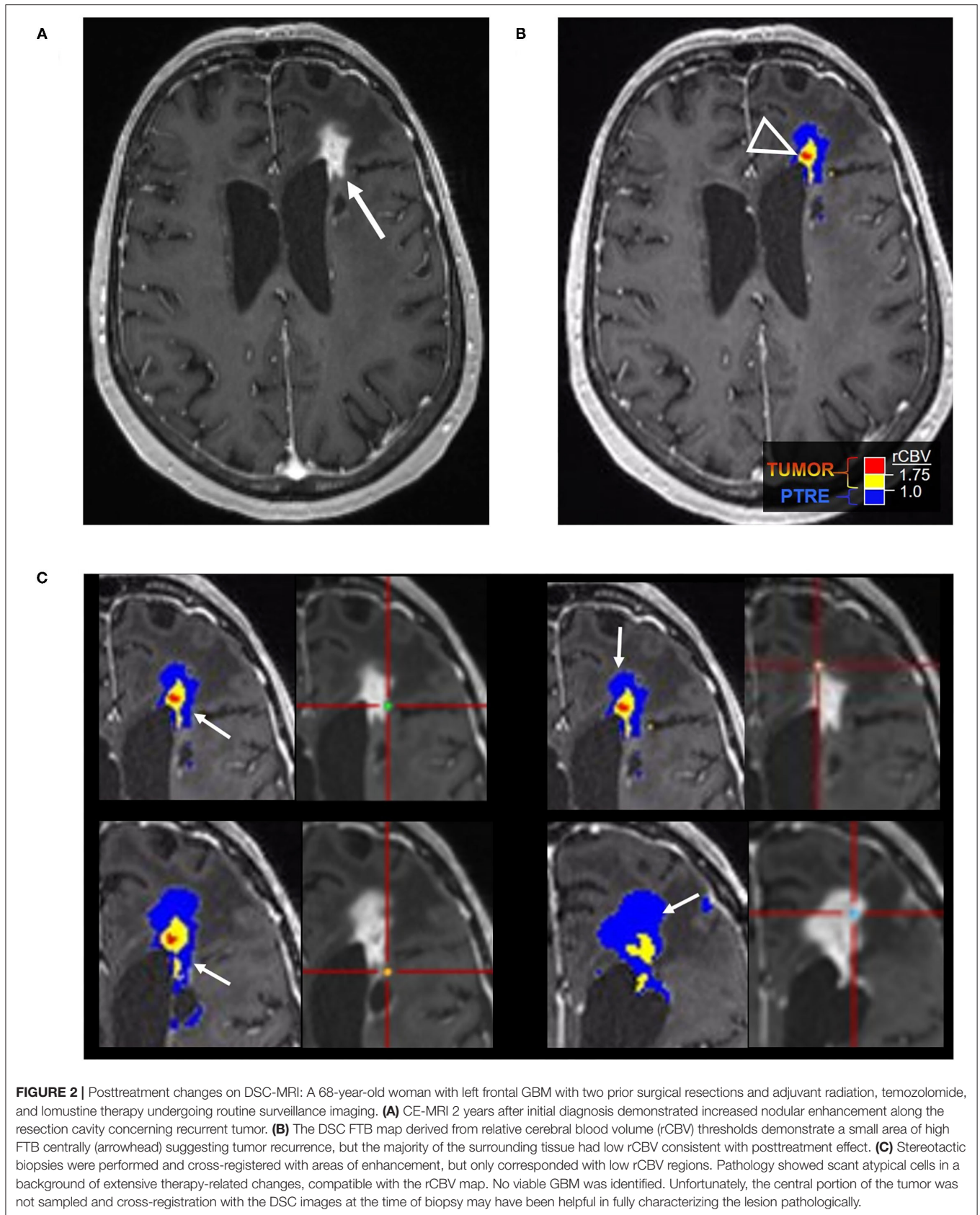
A second factor contributing to the variability in rCBV thresholds across published studies relates to differences in

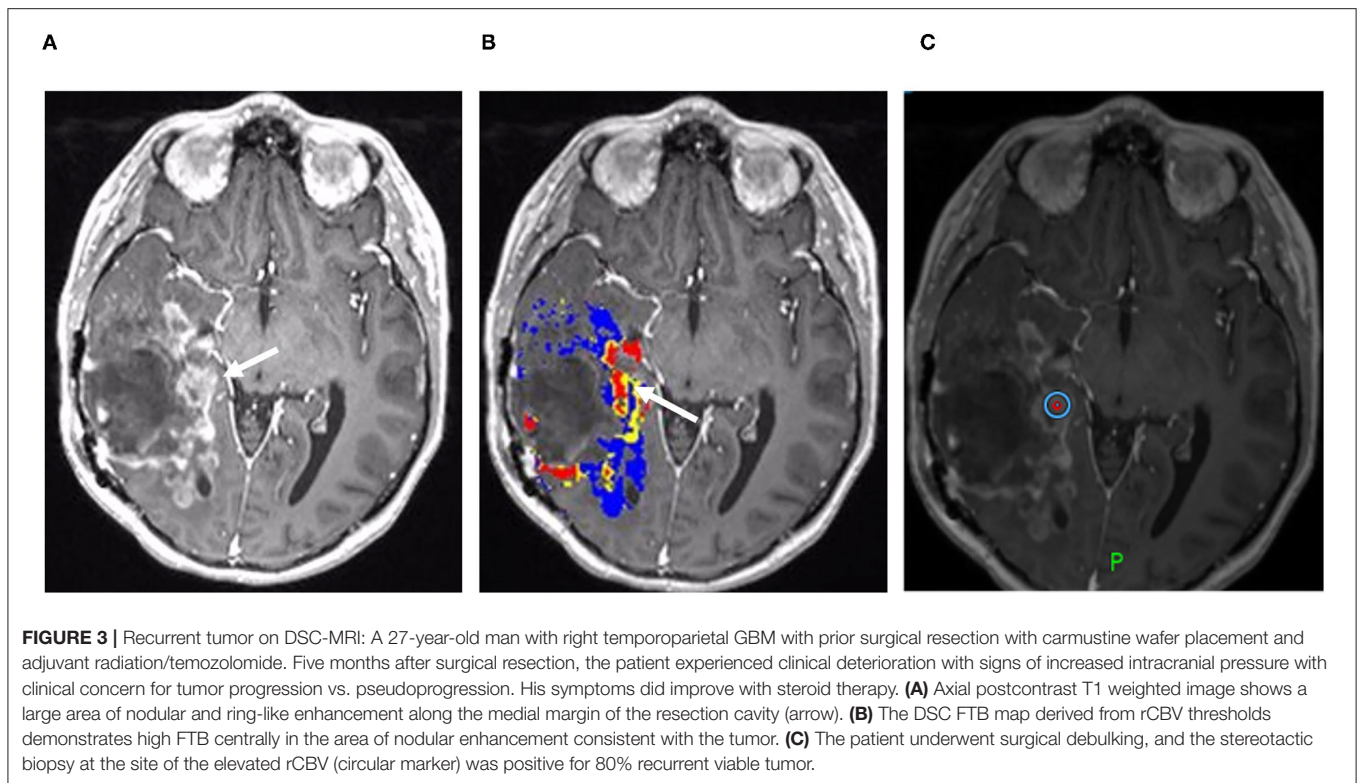


**FIGURE 1** | Posttreatment changes on Dynamic Susceptibility (DSC) MRI: A 58-year-old man with right frontal glioblastoma (GBM) status post resection and adjuvant radiation with concomitant temozolomide presented 6 months after resection with left facial droop and left-sided weakness. Initial CT and Contrast-enhanced MRI (CE-MRI) showed an increased mass effect and ill-defined enhancement around the resection cavity, indeterminate for recurrent tumor vs. posttreatment effects. **(A)** Axial postcontrast T1-weighted image demonstrates a linear enhancement around the right frontal resection cavity with more ill-defined nodular enhancement along the posteromedial margin (arrow). **(B)** Axial T2-weighted image shows T2 hyperintense signal and mass effect throughout the right frontal and parietal lobes. **(C)** DSC Fractional tumor burden (FTB) map derived from rCBV thresholds shows low FTB around the resection cavity favoring posttreatment changes **(D)** Stereotactic biopsies were performed and cross-registered retrospectively to areas of enhancement. Pathology demonstrated virtually entirely necrotic tissue with no viable tumor, concordant with the rCBV map.

the acquisition methods for clinical DSC-MRI. The meta-analysis by Patel et al. (68) highlighted the broad variability in pulse sequence parameters, principally the repetition time

(TR), echo time (TE), flip angle (FA), and contrast agent dosing. Variations in these pulse sequence parameters can affect the measurement of rCBV, particularly in the setting





of BBB disruption with resultant contrast extravasation, which can result in the so-called “T1W leakage effects” that lead to underestimates of rCBV (74). While T1W leakage effects are exaggerated by specific pulse sequence parameters (e.g., higher FA, a spin-echo technique), a number of studies have revealed techniques to minimize their influence. For instance, the use of preload bolus injection was introduced to “pre-saturate” T1W shortening prior to a second bolus injection for DSC-MRI acquisition (75, 76). A full-dose preload of 0.1 mmol/kg and the incubation time of 6 min in combination was found to optimize the differentiation of rCBVs between true tumor progression and PTREs, when validated against coregistered stereotactic biopsy specimens (77). The body of literature regarding the DSC-MRI accuracy has motivated the development and publication of consensus recommendations for DSC-MRI acquisition (57). This stemmed from initial efforts from the American Society of Functional Neuroradiology (ASFN), which released DSC protocol recommendations in 2015 prior to the BTIP consensus recommendations (78). Building upon the ASFN guidelines, the Jumpstarting Brain Tumor Drug Development Coalition Imaging Standardization Committee subsequently published the updated consensus recommendations for the DSC MRI protocol in 2020 (57). The consensus guidelines address the multiple protocol decisions that must be addressed for reliable CBV measurements. In addressing acquisition parameters, GRE sequences are recommended over spin echo, as the T2\*W effects of GRE are more sensitive to the larger vessels present in the gliomas. The GRE DSC effect is also proportional to GBCA concentration over a broader range

**TABLE 1 |** Consensus Guidelines for DSC MRI by Boxerman et al. (57).

Pulse sequence	Gradient echo
Mode	2D
Dosing protocol and flip angle (FA)	Pre-load + Bolus: 30° or 60° FA Bolus only: 30° FA
Echo time	3T: 30 ms (25–35 ms for 30° FA or 20–25 ms for 60° FA) 1.5T: 45 ms (40–50 ms)
Repetition time	1,000–1,500 ms
Total time points	≥120
Baseline time points	50 (30–50)

of vessel sizes, and GRE is less sensitive to changes in tissue-diffusion coefficient, which leads to greater rCBV accuracy. The recommended acquisition parameters, including the TR, TE, and FA, derived from computational studies aimed to optimize rCBV accuracy (79). The selected parameters were subsequently validated in patients. These parameters are summarized in **Table 1**.

A third factor contributing to variability in the published rCBV thresholds relates to the use of postprocessing model-based correction for rCBV measurements. Model-based postprocessing is required to calculate “corrected rCBV” values that account for both T1W leakage effects and T2\*W residual effects that may persist despite optimal DSC acquisition conditions (74, 77). A model-based correction has been shown necessary, in addition to



the use of specific pulse sequence acquisition parameters, to fully correct for T1W leakage effects (as well as confounding residual T2\*W\* effects) (57). While there are a wide variety of model-based correction methods, some of the commercially available studies have shown that not all software methods can generate reliable corrected rCBV values. At least, 16 different software packages were used across the 28 studies of Patel et al.'s (68) meta-analysis. Different software modeling and postprocessing algorithms impact the accuracy and reproducibility of perfusion imaging. For instance, Conte et al. (80) studied the intraobserver and interobserver variability of DSC and DCE interpretation of 20 patients with two different commercial software packages and different postprocessing choices. Good intraobserver and interobserver reproducibility was seen with the use of particular software, but only "fair to moderate" agreement was seen with different software applications (80). Hu et al. (81) evaluated leakage correction and the rCBV calculations of 52 patients using two different commercial software packages (IB Neuro from Imaging Biometrics and nordicICE from NordicNeuroLab). In 12 of the patients, the parameters were also validated with histologic benchmarks from stereotactic biopsies. The study concluded that the IB Neuro software was more accurate in diagnosing tumor vs. posttreatment effects. This has motivated efforts by the quantitative imaging network (QIN) to compare broader arrays of model-based correction methods to work toward consensus recommendations (82–84).

### Recommendations on rCBV Thresholds to Distinguish Tumor From PTRE Following Standard Chemo-Radiation Therapy

Based on the issues discussed above, we recommend that the selection of a numerical rCBV threshold, to clinically distinguish tumor from PTRE, should be based on those reported thresholds that have been spatially validated through the use of image-localized biopsies. Due to the regionally specific nature of this method of validation, the rCBV thresholds are more appropriately applied to distinguish tumor vs. PTRE at the regional voxel level, rather than for a global single mean value across an entire enhancing MRI lesion (49, 52). The threshold of 1.0 normalized rCBV has been validated by Hu et al. (49) and provides a straightforward guideline for differentiating tumor ( $rCBV > 1.0$ ) from PTRE ( $rCBV \leq 1.0$ ). This value is derived by "normalizing" rCBV against CBV from two regions of interest (ROIs), placed within the normal appearing white matter (NAWM) adjacent to the frontal horn, and also within the corona radiata in the deep frontoparietal region, as seen in the Supplemental On-Line Figure 1 by Hoxworth et al. (51). An early study by Hu et al. (61) reported a lower threshold ( $rCBV = 0.71$ ) by normalizing the CBV against both the NAWM and deep gray matter structures in the basal ganglia. As the gray matter structures can exhibit higher microvessel density compared to the white matter, using the gray matter to normalize CBV will by definition result in lower normalized rCBV values. A separate study by Hu et al. (77) found that NAWM demonstrated greater stability in CBV over multiple preload dose injections, compared to the normal gray matter structures. As a result, our recommendation is to follow the simpler approach of using

NAWM to normalize CBV and to use the rCBV threshold of 1.0. While this threshold was validated for distinguishing the biopsy samples with any amount of tumor (i.e., greater than 0% tumor) from biopsy samples with pure PTRE (i.e., 0% tumor), Prah et al. (52) performed a separate image-localized biopsy study and validated a similar rCBV threshold to distinguish the pure tumor (i.e., 100% tumor) from pure PTRE (i.e., 0% tumor) biopsy specimens. Of note, these rCBV thresholds are specific to postprocessing software (49, 51, 52, 81), and the thresholds may need to be modified if other postprocessing software methods are used. As an alternative to the normalization process, which requires the user-input to place NAWM ROIs, the use of standardized rCBV (std-rCBV) values has been proposed to help offset the potential variabilities in user-defined inputs (85). A std-rCBV threshold to distinguish tumor from PTRE was first validated by Prah et al. (52), employing the image-localized biopsies. The scale of the std-rCBV reported by Prah et al. (52) (3,575 a.u.) has since been modified to mirror the scale of normalized rCBV values (1.0 a.u.), and the threshold of 1.0 for std-rCBV was validated subsequently by Hoxworth et al. (51) using image-localized biopsies to reliably distinguish HGG recurrence PTRE. As such, our recommendation of the threshold of 1.0 can be used for both normalized rCBV and standardized rCBV measurements to distinguish the HGG recurrence from PTRE. This can be applied to measurable enhancing lesions both within and beyond the radiation field. Of note, these thresholds have not yet been validated for other tumor types, such as metastases or primary CNS lymphoma. Application of these thresholds for non-measurable disease (defined by RANO criteria) has also not been validated, particularly for non-enhancing T2/FLAIR regions, and should represent an important focus for future studies. With respect to non-measurable enhancing lesions, care should be taken not to "over-interpret" the rCBV maps in setting the small lesions (on the order of several millimeters), as the DSC-MRI technique has an inherent limitation to spatial resolution (voxel sizes in the order of several millimeters).

### Use of rCBV in the Setting of Anti-angiogenic Therapy

Anti-angiogenic therapies like bevacizumab demonstrate a strong effect on vessel permeability, which decreases as a result of the blockade in VEGF pathways. Post-processing leakage correction algorithms are particularly important in this setting, to offset potential technical influences of rCBV measurement that result from alterations in T1W leakage effects across serial examinations. Anti-angiogenic therapies also likely exert a measurable decrease in the microvessel volume, which has been shown in preclinical models to be due in part to pericyte contraction (86). Clinical studies utilizing dual-echo GE/SE DSC MRI before, during, and after anti-angiogenic therapy have shown decreased relative vessel size, particularly affecting large-caliber microvessels (those greater than 5–10 microns in diameter) (87). Despite these observed decreases in tumoral rCBV following anti-angiogenic therapy, longitudinal clinical trial data have shown that the rCBV values themselves, in many cases, do not necessarily fall below the spatially-validated thresholds for distinguishing tumor from PTRE (88), including

those for standardized rCBV (51, 52) and normalized rCBV (49). For example, if we were to consider the standardized rCBV threshold (greater than 3,575 a.u. represents tumor, less than 3,575 represents PTRE), as reported by Prah et al. (52) that was spatially validated using image-localized biopsies, then we observe that in **Figure 5A** of the study by Schmainda et al. (88), many of the lesions with elevated rCBV above the threshold (presumably representing tumor) on the pretreatment timepoint (TP1), continued to retain the elevated rCBV values above the threshold at the posttreatment time point (TP2). As such, despite a serial decrease in rCBV following anti-angiogenic therapy, an absolute rCBV value that remains above the threshold would still provide value in distinguishing HGG recurrence from PTRE. In contrast, for those lesions that demonstrated a fall in rCBV below the threshold following anti-angiogenic therapy, the rCBV would be non-specific for distinguishing the tumor (with diminished microvessel volume) from PTRE.

### Utility of DSC-MRI and RCBV to Distinguish Tumor From Pseudoprogression Following Immune Therapies

There have been preliminary studies evaluating the potential prognostic associations between rCBV and RANO-based classification of tumor progression vs. pseudoprogression in HGG following immune-based therapies (34, 89, 90). For instance, Cuccarini et al. (89) analyzed serial rCBV measurements following Dendritic Cell Immunotherapy and found that the serial increase in rCBV was correlated with the likelihood of tumor progression based on RANO criteria. However, similar to standard chemoradiation therapy, immune-based therapies can induce treatment-related changes that result in variable histologic admixture between pseudoprogression and tumor recurrence, with the possibility of a single MRI enhancing lesion demonstrating both the components of PTRE (that resolve over time) as well as components of tumor progression (that increase over time) (36, 53). This presents similar confounding limitations in RANO-based criteria as a surrogate for histologic identity and underscores the critical importance of establishing rCBV guidelines based on histologic validation from surgical tissue specimens using image-localized biopsies. To date, no published studies have validated the use of DSC-MRI metrics, including rCBV, to distinguish HGG recurrence from posttreatment-related effects following immune therapies. As such, no reliable thresholds can be recommended at this time. However, given the increasing use of immune-based therapies in the treatment of HGG, it is paramount to perform such histologic validation studies as a future goal in neuro-oncologic research. For such future studies, it would be important to adhere to consensus recommendations for DSC-MRI acquisition (57).

A potential alternative to gadolinium-based DSC-MRI uses ferumoxytol, an ultrasmall superparamagnetic iron oxide nanoparticle, which has been introduced as an off-label MRI contrast agent and does not extravasate due to its larger particle size (91–94). This technique has been used to distinguish pseudoprogression from tumor recurrence, and, with delayed imaging, provides additional information about neuro-inflammation, as it is phagocytosed by inflammatory

cells and potentially localizing cells, such as tumor-associated macrophages (95, 96). However, it is likely to be used in complement to gadolinium-based DSC MRI, as this contrast agent serves as the current clinical standard for CE-MRI in neuro-oncologic practice using the BTIP protocol. Also, there are potential issues, such as the time needed for the clearance of ferumoxytol, as MR image contrast may be altered by ferumoxytol for days to months after administration and by questions related to its safety profile (97).

### Utility of PSR and PH in Distinguishing HGG Recurrence From PTRE

Young et al. (66) evaluated a cohort of 20 patients with GBM, 9 of whom had pathologic confirmation, although not with spatially resolved image-localized biopsies. In the absence of pathologic specimens, they relied on imaging follow-up and RANO criteria to classify lesions as either tumor progression or as pseudoprogression. None of the pseudoprogression cases were confirmed by biopsy. Their DSC-MRI protocol employed a pulse sequence with the FA of 60 degrees, with no preload dose administration. They found that rCBV was significantly higher in the tumor progression group and that PSR was significantly lower in the tumor progression compared to the pseudoprogression group. They observed similar predictive accuracy when comparing the use of rCBV vs. PSR. In a larger cohort of 57 recurrent patients with GBM, Barajas et al. (72) also evaluated the predictive performance of rCBV, PH, and PSR derived from DSC-MRI (FA = 35 degrees, no preload dose). They were able to confirm PTRE in a larger number of patients (15 out of 17 cases) through validation by surgical biopsy specimens, although these were not spatially resolved using image-localized biopsies. They found that PH, like rCBV, was significantly increased in the tumor compared to the PTRE cases. Similar to the findings of Young et al. (66), they also found that PSR was significantly lower in tumor progression compared to higher PSR values in the PTRE group and that rCBV, PH, and PSR provided similar predictive performance in distinguishing tumors from PTRE (72). Prah et al. (52) compared PSR measurements in spatially localized biopsy specimens that confirmed regional diagnosis of tumor vs. PTRE. They found that rCBV outperformed PSR measurements and that PSR could not reliably distinguish tumor from PTRE. However, this study employed preload dose prior to PSR measurement, which has been shown to degrade the reliability of PSR as a predictive metric (98). As such, future studies employing image-localized biopsy specimens to validate PSR measurements should utilize DSC-MRI acquisitions in the absence of preload dose. An example case of PSR measurement is provided in **Figure 4**.

### Dynamic Contrast Enhanced Perfusion Imaging

DCE-MRI is based on the T1 relativity effects of gadolinium in contrast to the T1-weighted imaging before, during, and after contrast administration. The derived signal intensity-time curve depicts the influx of contrast agent into the local vasculature and its extravasation into the extravascular space (56). In brain tumors,  $K^{trans}$  is a derived volume transfer constant that primarily reflects capillary permeability by measuring the

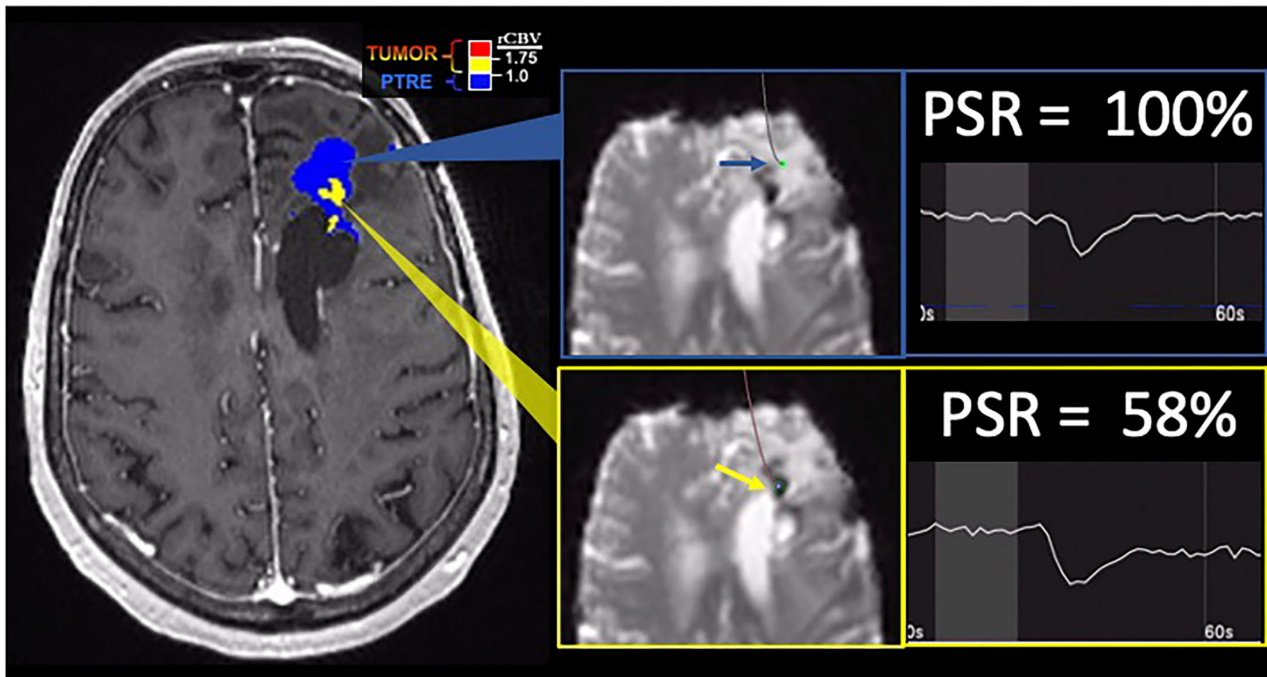


**FIGURE 4 |** Percentage signal recovery in PTRE and recurrent tumor: A 68-year-old woman with left frontal GBM with two prior surgical resections and adjuvant radiation, temozolomide, and lomustine therapy undergoing routine surveillance imaging. DSC was performed due to concern for tumor recurrence (refer to **Figure 2**). The FTB map shows peripheral low rCBV (blue) consistent with PTRE which was confirmed on stereotactic biopsy. The central component with higher rCBV (yellow) was presumed to have a recurrent tumor and resected, but not confirmed with stereotactic biopsy. Correlating PSR maps and signal intensity-time curves are provided to demonstrate a high PSR of essentially 100% for the peripheral region consistent with the PTRE and a lower PSR of 58% for the central region that was presumed to have a recurrent tumor.

transfer rate and accumulation of contrast in the extravascular extracellular space (EES). Additional derived parameters include  $v_e$ , a measure of the EES volume fraction, and  $v_p$ , the blood plasma volume fraction. Compared to DSC, fewer studies have evaluated DCE imaging for glioma follow-up, but  $K^{trans}$  is the most commonly reported parameter to differentiate tumor response from posttreatment effects (99–101). The 11 DCE studies that were included in the meta-analysis by Patel et al. (68) demonstrated a pooled sensitivity of 89% and specificity of 85%. Reported  $K^{trans}$  thresholds have a wide range (0.05–0.347) (99, 100), and this variability is caused by the same factors for variability discussed previously for DSC studies, including different quantitative models employed in the different certified software vendors. Furthermore, substantial inter-reader variability and lack of reproducibility have been reported with the use of DCE and  $K^{trans}$  (102).

Advantages of DCE (relative to DSC) include higher signal-to-noise ratio (SNR), spatial resolution, and reduced sensitivity to susceptibility artifacts (56). There are also fewer contamination effects from adjacent cortical/sulcal vessels, the calvarium, and the paranasal sinuses, which can be helpful in assessing the tumors near the cortical regions and the skull base. The complementary role of DCE in the case of hemosiderin deposition, which can cause artifacts on DSC, also supports the potential utility of using both DCE and DSC in

combination. Anzalone et al. (103) reported findings from a multi-center trial comparing DCE and DSC in the setting of pretreatment glioma grading and reported similar performance between the two techniques. However, the clinical translation of DCE has been hindered by several disadvantages, including longer acquisition time, fewer commercially available software packages, and far fewer validation studies comparing DCE metrics in the classification of tumor vs. PTRE. Additionally, DCE assessment of tumors is limited primarily due to the contrast-enhancing components (due to the dependency on BBB leakage). As such, the DCE shows limited applicability in assessing the non-enhancing components of tumors (compared to DSC-MRI). Finally, since DCE methods are less studied compared to the DSC, consensus efforts for standardization of acquisition/postprocessing are less developed. Future studies employing the histologic validation of DCE metrics, to differentiate tumor from PTRE, are needed, particularly taking into account the spatial heterogeneity through the use of image-localized biopsies.

### Arterial Spin Labeling

ASL represents an alternative perfusion imaging method that does not require exogenous gadolinium contrast agent administration. Tissue perfusion is measured by magnetically labeling the protons in the arterial blood using a 180-degree

radiofrequency inversion pulse on blood before it reaches the brain (104). The inversion pulse results in the magnetization of the water molecules in the blood which serve as an endogenous tracer that will alter the magnetization characteristics of the tissue of interest. The ASL data proportional to the cerebral blood flow is derived by subtracting the labeled images at the ROI from the control images prior to magnetic labeling. In evaluating brain tumors, cerebral blood flow (CBF) or tumor blood flow (TBF) is the most commonly reported parameter (105). In a study by Nyberg et al. (106), the authors reported a positive correlation between CBF from a region of interest across the entire MRI enhancing lesions and the histologic quantification of tumor (vs. PTRE elements) taken from a surgical resection material. While the ASL provides an alternative perfusion technique for patients when GBCA is contraindicated or not preferred (e.g., nephrogenic systemic fibrosis and pediatric populations), its widespread use has been limited by disadvantages, such as lower SNR, which increases the difficulty of clinical interpretation. Also, the vast majority of patients with HGG receive GBCA for routine CE-MRI examinations, which allows for DSC-MRI acquisition. Overall, there have been far fewer studies (compared to DSC-MRI) correlating ASL with the differentiation of tumor vs. PTRE (105–108). And to date, no studies have employed image-localized biopsies to directly compare the regional ASL measurements with spatially resolved histopathologic validation to address the confounds of intratumoral heterogeneity. While the ASL measures of CBF do not suffer from contrast agent leakage effects, they can be confounded by transit time delays (time between the tagging and acquisition of pulses) in tumors with highly tortuous vessels, and it is likely that CBF does not provide additional information above and beyond DSC-MRI measures of rCBV, particularly when appropriate acquisition and leakage correction methods are employed. As such, it is likely that the ASL continues to have a limited role for ASL in the routine clinical practice in the context of HGG response assessment.

## Metabolic MRI

Proton ( $^1\text{H}$ ) MRS is a method of metabolic assessment using the principle that different molecules resonate at slightly different frequencies and thus obtain different signal echoes. Given the significantly high relative ratio of water in the brain, water suppression must be performed with inversion recovery or chemical-shift selective techniques to provide resolution for the detection of these metabolites. These techniques require large volumes of interest for adequate SNR (43). Measurable metabolites include lactate, lipids, choline, glutamate, and 2-hydroxyglutarate. Choline (Cho), often present in cell membrane compounds, is associated with high cell turnover and tumor growth. Lactate can indicate tissue necrosis but is also present in tumor microenvironments by cells undergoing aerobic glycolysis (109). MRS has been shown to correlate with histologic findings in the initial workup of untreated disease, including identifying the molecular signatures of IDH mutations with increased levels of 2-hydroxyglutarate (110) and defining the tumor boundaries (111).

In posttreatment imaging, MRS has shown reasonable accuracy in distinguishing pure tumor or pure necrosis but has

limited accuracy in the setting of admixed histology (112). In a well-designed study by Rock et al. (112) employing image-localized biopsies and co-registered MRS measurements in a cohort of 27 recurrent HGG patients, it was found that a Cho to Creatine (Cr) ratio of 1.79 or greater provided 7 times the odds ratio of a biopsy sample yielding pure tumor (compared to pure PTRE). Unfortunately, no values of the MRS ratio could distinguish mixed specimens (containing both tumor and PTRE) in a statistically significant way from either pure tumor or pure PTRE. In a subsequent follow-up study from the same group, Rock et al. (113) reported a further refined Cho-to-Cr ratio threshold of 2.23 that could discriminate the pure tumor from pure PTRE with an odds ratio of 13.56. However, they again found that no MRS ratios could reliably distinguish the admixed specimens from a pure tumor or pure PTRE. Given that histologic heterogeneity commonly occurs in the setting of posttreatment HGG, and the need for large voxel volumes to maximize SNR ratio and the quality of MRS images, the MRS technique has suffered from declining clinical use. MRS also has the disadvantages of technically challenging imaging acquisitions, due to the need to avoid specific anatomic structures (i.e., ventricles, resection cavities, and scalp fat). As such, the scan time can be long if multiple repeated attempts for image acquisition are needed during a clinical examination. While multi-voxel MRS techniques have shown promise in differentiating the treatment recurrence vs. pseudoprogression, (114) this can further reduce SNR and further degrade the image quality, making the clinical interpretation difficult. As such, given the requirements of voxel size, the technical challenges of image acquisition, and the difficulty in assessing the intratumoral heterogeneity, the use of MRS is likely to remain secondary to techniques such as DSC-MRI. Nonetheless, metabolic information can potentially be complementary for specific clinical scenarios, such as the assessment of non-enhancing tumor regions (Figure 5).

## Machine Learning (ML), Deep Learning (DL), and Advanced Processing Methods for Distinguishing the Tumor Recurrence From PTRE

The field of radiomics has seen extensive growth in the past decade in medical imaging and typically employs a combination of image feature extraction (often through texture analysis) and ML/DL based approaches to develop predictive models for the characterization of diseases, such as glioma (46, 115). Most published studies have focused on the characterization of brain tumors prior to treatment, for instance, to predict the molecular subtypes or disease extent (116, 117). While a detailed discussion of the radiomics methods is beyond the scope of this review, which focuses primarily on perfusion and metabolic MRI, prior studies have applied these methods to help distinguish the tumor from PTRE in the posttreatment setting (118, 119). Other advanced postprocessing methods, such as the use of delayed contrast extravasation, have also been reported to help differentiate the lesions classified as tumor progression vs. pseudoprogression (120). In each of these circumstances, future studies are needed for validation, specifically with the use of spatially resolved image-localized biopsies to help overcome the

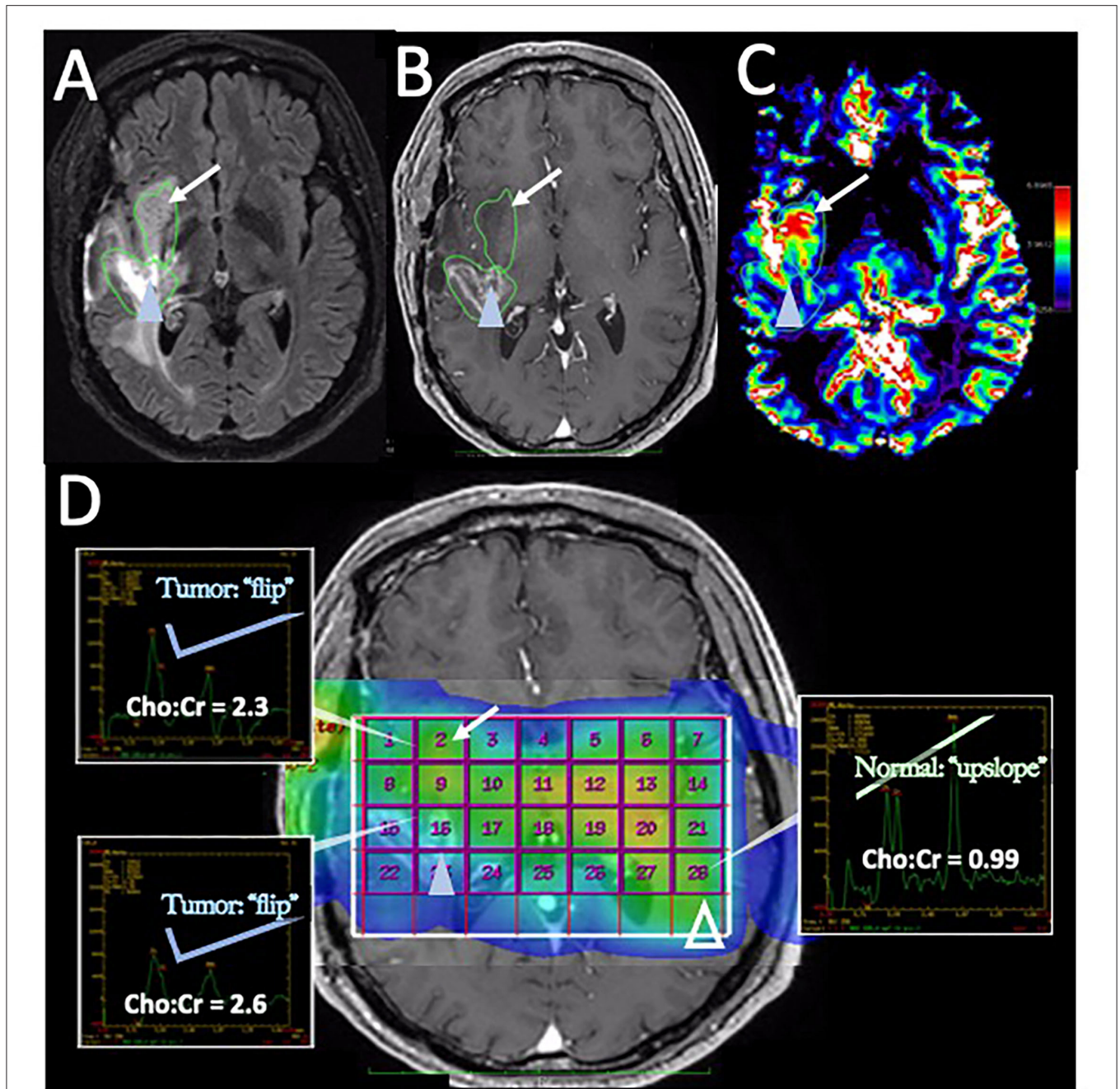


**FIGURE 5 |** Disease recurrence on DSC-MRI and MRS: A 50-year-old man with right temporal WHO grade III anaplastic oligodendroglioma status post three surgical resections, radiation therapy, and chemotherapy with temozolomide, procarbazine, and lomustine was found to have signs of recurrence on surveillance CE-MRI. **(A)** Axial FLAIR image superior to the resection cavity shows prominent increased FLAIR signal posteriorly (blue arrowhead) and less intense, but more rounded FLAIR signal anteriorly (arrow). **(B)** Axial post-contrast T1-weighted image demonstrates heterogeneous enhancement of the posterior region (blue arrowhead) with no significant enhancement in the anterior region (arrow). **(C)** The DSC rCBV map shows increased perfusion of the anterior nonenhancing/FLAIR hyperintense region (arrow) but heterogeneous areas of both increased and decreased perfusion in the enhancing posterior region (arrowhead). **(D)** Magnetic resonance spectroscopy (MRS) demonstrates elevated Cho:Cr ratios in both the anterior nonenhancing (arrow, ratio = 2.3) and the posterior enhancing (solid blue arrowhead, ratio = 2.6) regions. Normal ratios are shown on the contralateral brain (open arrowhead, Cho:Cr ratio = 0.99) for comparison, showing the normal upslope vs. the “Cho-to-Cr flip” seen with the tumor. Both sites with elevated Cho:Cr ratio was concerning for disease progression. The heterogeneous rCBV of the posterior enhancing region was attributed to a combination of disease recurrence and necrotic change. The patient was treated with repeat proton-beam radiation and temozolomide with improvement in the enhancement and FLAIR signal abnormality on subsequent MRI (not shown).

**TABLE 2 |** Summary of advanced MRI techniques and recommended thresholds for clinical use.

Imaging technique	Imaging metric	Tumor	PTRE	Premise	Limitations of technique	Reported thresholds from validation studies employing image-localized biopsies					
						Threshold	Sensitivity	Specificity	Accuracy	Study	Notes
<b>Summary of advanced MRI techniques</b>											
DSC-MRI	Normalized rCBV	High	Low	Microvessel volume	Susceptibility from blood products, large cortical vessels can obscure superficial regions	0.71	91.70%	100%	95.90%	Hu et al. (61)	Lower threshold results from normalizing to both NAWM and NAGM; tumor samples could be admixed
						1	100%	100%	100%	Hu et al. (49)	Normalized using only NAWM; only GBM specimens; tumor samples could be admixed
						1.13	82.10%	90%	86%	Prah et al. (52)	Pure GBM vs. pure PTRE; normalized using only NAWM
	Standardized rCBV	High	Low	Microvessel volume		3,575	79.40%	90%	84.70%	Prah et al. (52)	Pure GBM vs. pure PTRE
	Normalized cerebral blood flow	High	Low	Blood flow		1.05	79.40%	80%	79.70%	Prah et al. (52)	Pure GBM vs. pure PTRE
ASL	Cerebral blood flow	High	Low	Blood flow	May suffer from noisy maps due to limitations in SNR	NA					NA = not available, as validation studies employing image-localized biopsies have not been published
						NA					NA = not available, as validation studies employing image-localized biopsies have not been published
						NA					NA = not available, as validation studies employing image-localized biopsies have not been published
DCE-MRI	k-trans	High	Low	Vessel leakage	Longer acquisition time, fewer commercially available software packages, limited applicability for evaluating non-enhancing tumor	NA					NA = not available, as validation studies employing image-localized biopsies have not been published
						NA					NA = not available, as validation studies employing image-localized biopsies have not been published
MRS	Cho:Cr ratio	High	Low	High cellular membrane turnover	Large voxel volumes required to maximize SNR, limited ability to evaluate regions of histologic admixture between tumor and PTRE; technical challenges in image acquisition	Threshold	Odds ratio pure tumor (vs. pure PTRE)		Study	Notes	
						1.79	7		Rock et al. (112)	Pure tumor vs. pure PTRE	
						2.23	13.56		Rock et al. (113)	pure tumor vs. pure PTRE	

intratumoral heterogeneity and histologic admixture which can confound a diagnostic performance.

## SUMMARY AND FUTURE DIRECTIONS

Of the advanced imaging methods discussed, the DSC-MRI technique, specifically the measurement of rCBV, provides the most robust and widespread clinically adopted method for response assessment in HGG. For a summary the advanced MRI techniques discussed in this review, please refer to **Table 2**. This is due in large part to the myriad of published studies consistently demonstrating the high accuracy of rCBV to distinguish the tumor recurrence from PTRE, which represents a persisting clinical challenge for routine CE-MRI. With that said, there remains a need to develop consensus criteria for rCBV thresholds that will guide prospective clinical diagnosis of tumor vs. non-tumoral PTRE. There are several necessary gaps that will need to be addressed to facilitate the development of these diagnostic criteria. One important step has already been addressed, which is the development and publication of consensus recommendations on DSC-MRI acquisition methods (57). One immediate next step will necessitate multi-institutional clinical trials comparing rCBV measurements across clinical sites employing the consensus of DSC-MRI protocols. There is also a need for the development and validation of evidence-based consensus recommendations on model-based correction methods for the calculation of rCBV values, particularly in the context of correcting for T1W leakage effects (and residual T2\*W effects). This will need to be driven by clinical validation

studies employing spatially resolved histologic benchmarks (i.e., image-localized biopsy confirmation of tumor vs. PTRE). In this context, it will be critical to rely on validation techniques, namely image-localized biopsies, to provide spatially resolved datasets of localized rCBV measurements against spatially correlated histologic diagnosis. Given these spatially matched datasets, different leakage correction algorithms can be compared methodologically against one another to support consensus studies on model-based methods, as well as the corresponding rCBV threshold criteria (that may be specific to model-based correction methods) to guide prospective clinical diagnosis. Finally, there remains the need for further studies to understand the potential utility in quantifying tumor burden relative to PTRE in those lesions with histologic admixture. This may help refine clinical diagnostic criteria for response assessment and prognostication and to provide quantitative methods to assess the efficacy of future novel therapeutic strategies.

## AUTHOR CONTRIBUTIONS

All authors listed have made a substantial, direct, and intellectual contribution to the work and approved it for publication.

## FUNDING

U01 CA250481, U01 CA220378, R01 CA221938, R01 CA158079-01, and U01 CA176110 funded co-author effort and data acquisition/analysis. Mayo Clinic Foundation provided funding for open access publication fees.

## REFERENCES

- National Comprehensive Cancer Network. Central Nervous System Cancers. (Version 2.2021). Available online at: [https://www.nccn.org/professionals/physician\\_gls/pdf/cns.pdf](https://www.nccn.org/professionals/physician_gls/pdf/cns.pdf) (accessed October 7, 2021).
- Ellingson BM, Bendszus M, Boxerman J, Barboriak D, Erickson BJ, Smits M, et al. Consensus recommendations for a standardized brain tumor imaging protocol in clinical trials. *Neuro Oncol.* (2015) 17:1188–98. doi: 10.1093/neuonc/nov095
- Verma N, Cowperthwaite MC, Burnett MG, Markey MK. Differentiating tumor recurrence from treatment necrosis: a review of neuro-oncologic imaging strategies. *Neuro Oncol.* (2013) 15:515–34. doi: 10.1093/neuonc/nos307
- Walker MD, Alexander E Jr, Hunt WE, MacCarty CS, Mahaley MS Jr, Mealey J Jr, et al. Evaluation of BCNU and/or radiotherapy in the treatment of anaplastic gliomas. A cooperative clinical trial: a cooperative clinical trial. *J Neurosurg.* (1978) 49:333–43. doi: 10.3171/jns.1978.49.3.0333
- Stupp R, Mason WP, van den Bent MJ, Weller M, Fisher B, Taphoorn MJB, et al. Radiotherapy plus concomitant and adjuvant temozolomide for glioblastoma. *N Engl J Med.* (2005) 352:987–96. doi: 10.1056/NEJMoa043330
- Fisher JB, Adamson DC. Current FDA-approved therapies for high-grade malignant gliomas. *Biomedicine.* (2021) 9:324. doi: 10.3390/biomedicine9030324
- Wenger KJ, Wagner M, You S-J, Franz K, Harter PN, Burger MC, et al. Bevacizumab as a last-line treatment for glioblastoma following failure of radiotherapy, temozolomide and lomustine. *Oncol Lett.* (2017) 14:1141–6. doi: 10.3892/ol.2017.6251
- Brandsma D, van den Bent MJ. Pseudoprogression and pseudoresponse in the treatment of gliomas. *Curr Opin Neurol.* (2009) 22:633–8. doi: 10.1097/WCO.0b013e3283232363e
- Xu S, Tang L, Li X, Fan F, Liu Z. Immunotherapy for glioma: current management and future application. *Cancer Lett.* (2020) 476:1–12. doi: 10.1016/j.canlet.2020.02.002
- Huang B, Li X, Li Y, Zhang J, Zong Z, Zhang H. Current immunotherapies for glioblastoma multiforme. *Front Immunol.* (2020) 11:603911. doi: 10.3389/fimmu.2020.603911
- Fecci PE, Ochiai H, Mitchell DA, Grossi PM, Sweeney AE, Archer GE, et al. Systemic CTLA-4 blockade ameliorates glioma-induced changes to the CD4+ T cell compartment without affecting regulatory T-cell function. *Clin Cancer Res.* (2007) 13:2158–67. doi: 10.1158/1078-0432.CCR-06-2070
- Zeng J, See AP, Phallen J, Jackson CM, Belcaid Z, Ruzevick J, et al. Anti-PD-1 blockade and stereotactic radiation produce long-term survival in mice with intracranial gliomas. *Int J Radiat Oncol Biol Phys.* (2013) 86:343–9. doi: 10.1016/j.ijrobp.2012.12.025
- Wheeler CJ, Black KL, Liu G, Mazer M, Zhang X-X, Pepkowitz S, et al. Vaccination elicits correlated immune and clinical responses in glioblastoma multiforme patients. *Cancer Res.* (2008) 68:5955–64. doi: 10.1158/0008-5472.CAN-07-5973
- Schaller TH, Sampson JH. Advances and challenges: dendritic cell vaccination strategies for glioblastoma. *Exp Rev Vaccines.* (2017) 16:27–36. doi: 10.1080/14760584.2016.1218762
- Nehama D, Di Ianni N, Musio S, Du H, Patané M, Pollo B, et al. B7-H3-redirected chimeric antigen receptor T cells target glioblastoma and neurospheres. *EBioMedicine.* (2019) 47:33–43. doi: 10.1016/j.ebiom.2019.08.030
- Brown CE, Alizadeh D, Starr R, Weng L, Wagner JR, Naranjo A, et al. Regression of glioblastoma after chimeric antigen receptor T-cell therapy. *N Engl J Med.* (2016) 375:2561–9. doi: 10.1056/NEJMoa1610497
- Brandsma D, Stalpers L, Taal W, Sminia P, van den Bent MJ. Clinical features, mechanisms, and management of pseudoprogression in malignant

- gliomas. *Lancet Oncol.* (2008) 9:453–61. doi: 10.1016/S1470-2045(08)70125-6
18. Thust SC, van den Bent MJ, Smits M. Pseudoprogression of brain tumors: pseudoprogression of Brain Tumors. *J Magn Reson Imaging.* (2018) 48:571–89. doi: 10.1002/jmri.26171
  19. Ellingson BM, Chung C, Pope WB, Boxerman JL, Kaufmann TJ. Pseudoprogression, radionecrosis, inflammation or true tumor progression? Challenges associated with glioblastoma response assessment in an evolving therapeutic landscape. *J Neurooncol.* (2017) 134:495–504. doi: 10.1007/s11060-017-2375-2
  20. Miyatake S-I, Nonoguchi N, Furuse M, Yoritsune E, Miyata T, Kawabata S, et al. Pathophysiology, diagnosis, and treatment of radiation necrosis in the brain. *Neurol Med Chir.* (2015) 55:50–9. doi: 10.2176/nmc.ra.2014-0188
  21. de Wit MCY, de Bruin HG, Eijkenboom W, Sillevs Smitt PAE, van den Bent MJ. Immediate post-radiotherapy changes in malignant glioma can mimic tumor progression. *Neurology.* (2004) 63:535–7. doi: 10.1212/01.wnl.0000133398.11870.9a
  22. Gerstner ER, McNamara MB, Norden AD, Lafrankie D, Wen PY. Effect of adding temozolomide to radiation therapy on the incidence of pseudo-progression. *J Neurooncol.* (2009) 94:97–101. doi: 10.1007/s11060-009-9809-4
  23. Chamberlain MC, Glantz MJ, Chalmers L, Van Horn A, Sloan AE. Early necrosis following concurrent Temodar and radiotherapy in patients with glioblastoma. *J Neurooncol.* (2007) 82:81–3. doi: 10.1007/s11060-006-9241-y
  24. Bobola MS, Kolstoe DD, Blank A, Silber JR. Minimally cytotoxic doses of temozolomide produce radiosensitization in human glioblastoma cells regardless of MGMT expression. *Mol Cancer Ther.* (2010) 9:1208–18. doi: 10.1158/1535-7163.MCT-10-0010
  25. Gahramanov S, Varallyay C, Tyson RM, Lacy C, Fu R, Netto JP, et al. Diagnosis of pseudoprogression using MRI perfusion in patients with glioblastoma multiforme may predict improved survival. *CNS Oncol.* (2014) 3:389–400. doi: 10.2217/cns.14.42
  26. Bronk JK, Guha-Thakurta N, Allen PK, Mahajan A, Grosshans DR, McGovern SL. Analysis of pseudoprogression after proton or photon therapy of 99 patients with low grade and anaplastic glioma. *Clin Transl Radiat Oncol.* (2018) 9:30–4. doi: 10.1016/j.ctro.2018.01.002
  27. Brandes AA, Franceschi E, Tosoni A, Blatt V, Pession A, Tallini G, et al. MGMT promoter methylation status can predict the incidence and outcome of pseudoprogression after concomitant radiochemotherapy in newly diagnosed glioblastoma patients. *J Clin Oncol.* (2008) 26:2192–7. doi: 10.1200/JCO.2007.14.8163
  28. McGirt MJ, Bulsara KR, Cummings TJ, New KC, Little KM, Friedman HS, et al. Prognostic value of magnetic resonance imaging-guided stereotactic biopsy in the evaluation of recurrent malignant astrocytoma compared with a lesion due to radiation effect. *J Neurosurg.* (2003) 98:14–20. doi: 10.3171/jns.2003.98.1.0014
  29. Himes BT, Arnett AL, Merrell KW, Gates MJ, Bhargav AG, Raghunathan A, et al. Glioblastoma recurrence versus treatment effect in a pathology-documented series. *Can J Neurol Sci.* (2020) 47:525–30. doi: 10.1017/cjn.2020.36
  30. Hygino da Cruz LC Jr, Rodriguez I, Domingues RC, Gasparetto EL, Sorensen AG. Pseudoprogression and pseudoresponse: imaging challenges in the assessment of posttreatment glioma. *AJNR Am J Neuroradiol.* (2011) 32:1978–85. doi: 10.3174/ajnr.A2397
  31. Melguizo-Gavilanes I, Bruner JM, Guha-Thakurta N, Hess KR, Puduvalli VK. Characterization of pseudoprogression in patients with glioblastoma: is histology the gold standard? *J Neurooncol.* (2015) 123:141–50. doi: 10.1007/s11060-015-1774-5
  32. Abbasi AW, Westerlaan HE, Holtman GA, Aden KM, van Laar PJ, van der Hoorn A. Incidence of tumour progression and pseudoprogression in high-grade gliomas: a systematic review and meta-analysis. *Clin Neuroradiol.* (2018) 28:401–11. doi: 10.1007/s00062-017-0584-x
  33. Parvez K, Parvez A, Zadeh G. The diagnosis and treatment of pseudoprogression, radiation necrosis and brain tumor recurrence. *Int J Mol Sci.* (2014) 15:11832–46. doi: 10.3390/ijms150711832
  34. Song J, Kadaba P, Kravitz A, Hormigo A, Friedman J, Belani P, et al. Multiparametric MRI for early identification of therapeutic response in recurrent glioblastoma treated with immune checkpoint inhibitors. *Neuro Oncol.* (2020) 22:1658–66. doi: 10.1093/neuonc/noaa066
  35. Jia W, Gao Q, Han A, Zhu H, Yu J. The potential mechanism, recognition and clinical significance of tumor pseudoprogression after immunotherapy. *Cancer Biol Med.* (2019) 16:655–70. doi: 10.20892/j.issn.2095-3941.2019.0144
  36. Okada H, Weller M, Huang R, Finocchiaro G, Gilbert MR, Wick W, et al. Immunotherapy response assessment in neuro-oncology: a report of the RANO working group. *Lancet Oncol.* (2015) 16:e534–42. doi: 10.1016/S1470-2045(15)00088-1
  37. Cohen JV, Alomari AK, Vortmeyer AO, Jilaveanu LB, Goldberg SB, Mahajan A, et al. Melanoma brain metastasis pseudoprogression after pembrolizumab treatment. *Cancer Immunol Res.* (2016) 4:179–82. doi: 10.1158/2326-6066.CIR-15-0160
  38. Gatson NTN, Makary M, Bross SP, Vadakara J, Maiers T, Mongelluzzo GJ, et al. Case series review of neuroradiologic changes associated with immune checkpoint inhibitor therapy. *Neurooncol Pract.* (2021) 8:247–58. doi: 10.1093/nop/npaa079
  39. Johnson DB, Manouchehri A, Haugh AM, Quach HT, Balko JM, Lebrun-Vignes B, et al. Neurologic toxicity associated with immune checkpoint inhibitors: a pharmacovigilance study. *J Immunother Cancer.* (2019) 7:134. doi: 10.1186/s40425-019-0617-x
  40. Spain L, Walls G, Julve M, O'Meara K, Schmid T, Kalaitzaki E, et al. Neurotoxicity from immune-checkpoint inhibition in the treatment of melanoma: a single centre experience and review of the literature. *Ann Oncol.* (2017) 28:377–85. doi: 10.1093/annonc/mdw558
  41. Albert FK, Forsting M, Sartor K, Adams H-P, Kunze S. Early postoperative magnetic resonance imaging after resection of malignant glioma: objective evaluation of residual tumor and its influence on regrowth and prognosis. *Neurosurgery.* (1994) 34:45–61. doi: 10.1227/00006123-199401000-00008
  42. Macdonald DR, Cascino TL, Schold SC Jr, Cairncross JG. Response criteria for phase II studies of supratentorial malignant glioma. *J Clin Oncol.* (1990) 8:1277–80. doi: 10.1200/JCO.1990.8.1277
  43. Wen PY, Macdonald DR, Reardon DA, Cloughesy TF, Sorensen AG, Galanis E, et al. Updated response assessment criteria for high-grade gliomas: response assessment in neuro-oncology working group. *J Clin Oncol.* (2010) 28:1963–72. doi: 10.1200/JCO.2009.26.3541
  44. Ellingson BM, Wen PY, Cloughesy TF. Modified criteria for radiographic response assessment in glioblastoma clinical trials. *Neurotherapeutics.* (2017) 14:307–20. doi: 10.1007/s13311-016-0507-6
  45. Dubois LG, Campanati L, Righy C, D'Andrea-Meira I, Spohr TCL de SE, Porto-Carreiro I, et al. Gliomas and the vascular fragility of the blood brain barrier. *Front Cell Neurosci.* (2014) 8:418. doi: 10.3389/fncel.2014.00418
  46. Hu LS, Hawkins-Daarud A, Wang L, Li J, Swanson KR. Imaging of intratumoral heterogeneity in high-grade glioma. *Cancer Lett.* (2020) 477:97–106. doi: 10.1016/j.canlet.2020.02.025
  47. Kumar AJ, Leeds NE, Fuller GN, Van Tassel P, Maor MH, Sawaya RE, et al. Malignant gliomas: MR imaging spectrum of radiation therapy- and chemotherapy-induced necrosis of the brain after treatment. *Radiology.* (2000) 217:377–84. doi: 10.1148/radiology.217.2.r00nv36377
  48. Tihan T, Barletta J, Parney I, Lamborn K, Sneed PK, Chang S. Prognostic value of detecting recurrent glioblastoma multiforme in surgical specimens from patients after radiotherapy: should pathology evaluation alter treatment decisions? *Hum Pathol.* (2006) 37:272–82. doi: 10.1016/j.humpath.2005.11.010
  49. Hu LS, Eschbacher JM, Heiserman JE, Dueck AC, Shapiro WR, Liu S, et al. Reevaluating the imaging definition of tumor progression: perfusion MRI quantifies recurrent glioblastoma tumor fraction, pseudoprogression, and radiation necrosis to predict survival. *Neuro Oncol.* (2012) 14:919–30. doi: 10.1093/neuonc/nos112
  50. Winter SF, Vaio EJ, Muzikansky A, Martinez-Lage M, Bussièrè MR, Shih HA, et al. Defining treatment-related adverse effects in patients with glioma: distinctive features of pseudoprogression and treatment-induced necrosis. *Oncologist.* (2020) 25:e1221–32. doi: 10.1634/theoncologist.2020-0085
  51. Hoxworth JM, Eschbacher JM, Gonzales AC, Singleton KW, Leon GD, Smith KA, et al. Performance of standardized relative CBV for quantifying regional histologic tumor burden in recurrent high-grade glioma: comparison against



- normalized relative CBV using image-localized stereotactic biopsies. *AJNR Am J Neuroradiol.* (2020) 41:408–15. doi: 10.3174/ajnr.A6486
52. Prah MA, Al-Gizawiy MM, Mueller WM, Cochran EJ, Hoffmann RG, Connelly JM, et al. Spatial discrimination of glioblastoma and treatment effect with histologically-validated perfusion and diffusion magnetic resonance imaging metrics. *J Neurooncol.* (2018) 136:13–21. doi: 10.1007/s11060-017-2617-3
  53. Furtado AD, Ceschin R, Blüml S, Mason G, Jakacki RI, Okada H, et al. Neuroimaging of peptide-based vaccine therapy in pediatric brain tumors: initial experience. *Neuroimaging Clin N Am.* (2017) 27:155–66. doi: 10.1016/j.nic.2016.09.002
  54. Forsyth PA, Kelly PJ, Cascino TL, Scheithauer BW, Shaw EG, Dinapoli RP, et al. Radiation necrosis or glioma recurrence: is computer-assisted stereotactic biopsy useful? *J Neurosurg.* (1995) 82:436–44. doi: 10.3171/jns.1995.82.3.0436
  55. Bagley SJ, Schwab RD, Nelson E, Viaene AN, Binder ZA, Lustig RA, et al. Histopathologic quantification of viable tumor versus treatment effect in surgically resected recurrent glioblastoma. *J Neurooncol.* (2019) 141:421–9. doi: 10.1007/s11060-018-03050-6
  56. Essig M, Shiroishi MS, Nguyen TB, Saake M, Provenzale JM, Enterline D, et al. Perfusion MRI: the five most frequently asked technical questions. *AJR Am J Roentgenol.* (2013) 200:24–34. doi: 10.2214/AJR.12.9543
  57. Boxerman JL, Quarles CC, Hu LS, Erickson BJ, Gerstner ER, Smits M, et al. Consensus recommendations for a dynamic susceptibility contrast MRI protocol for use in high-grade gliomas. *Neuro Oncol.* (2020) 22:1262–75. doi: 10.1093/neuonc/noaa141
  58. Cha S, Lu S, Johnson G, Knopp EA. Dynamic susceptibility contrast MR imaging: correlation of signal intensity changes with cerebral blood volume measurements. *J Magn Reson Imaging.* (2000) 11:114–9. doi: 10.1002/(sici)1522-2586(200002)11:2<114::aid-jmri6>3.0.co;2-s
  59. Cha S, Lupo JM, Chen M-H, Lamborn KR, McDermott MW, Berger MS, et al. Differentiation of glioblastoma multiforme and single brain metastasis by peak height and percentage of signal intensity recovery derived from dynamic susceptibility-weighted contrast-enhanced perfusion MR imaging. *AJNR Am J Neuroradiol.* (2007) 28:1078–84. doi: 10.3174/ajnr.A0484
  60. Hu LS, Eschbacher JM, Dueck AC, Heiserman JE, Liu S, Karis JP, et al. Correlations between perfusion MR imaging cerebral blood volume, microvessel quantification, and clinical outcome using stereotactic analysis in recurrent high-grade glioma. *AJNR Am J Neuroradiol.* (2012) 33:69–76. doi: 10.3174/ajnr.A2743
  61. Hu LS, Baxter LC, Smith KA, Feuerstein BG, Karis JP, Eschbacher JM, et al. Relative cerebral blood volume values to differentiate high-grade glioma recurrence from posttreatment radiation effect: direct correlation between image-guided tissue histopathology and localized dynamic susceptibility-weighted contrast-enhanced perfusion MR imaging measurements. *AJNR Am J Neuroradiol.* (2009) 30:552–8. doi: 10.3174/ajnr.A1377
  62. Mangla R, Singh G, Ziegler D, Milano MT, Korones DN, Zhong J, et al. Changes in relative cerebral blood volume 1 month after radiation-temozolomide therapy can help predict overall survival in patients with glioblastoma. *Radiology.* (2010) 256:575–84. doi: 10.1148/radiol.10091440
  63. Alexiou GA, Zikou A, Tsiouris S, Goussia A, Kosta P, Papadopoulos A, et al. Comparison of diffusion tensor, dynamic susceptibility contrast MRI and (99m)Tc-Tetrofosmin brain SPECT for the detection of recurrent high-grade glioma. *Magn Reson Imaging.* (2014) 32:854–9. doi: 10.1016/j.mri.2014.04.013
  64. Gasparetto EL, Pawlak MA, Patel SH, Huse J, Woo JH, Krejza J, et al. Posttreatment recurrence of malignant brain neoplasm: accuracy of relative cerebral blood volume fraction in discriminating low from high malignant histologic volume fraction. *Radiology.* (2009) 250:887–96. doi: 10.1148/radiol.2502071444
  65. Martínez-Martínez A, Martínez-Bosch J. Perfusion magnetic resonance imaging for high grade astrocytomas: can cerebral blood volume, peak height, and percentage of signal intensity recovery distinguish between progression and pseudoprogression? *Radiol (Engl Ed).* (2014) 56:35–43. doi: 10.1016/j.rxe.2014.02.003
  66. Young RJ, Gupta A, Shah AD, Graber JJ, Chan TA, Zhang Z, et al. MRI perfusion in determining pseudoprogression in patients with glioblastoma. *Clin Imaging.* (2013) 37:41–9. doi: 10.1016/j.clinimag.2012.02.016
  67. Kim HS, Suh CH, Kim N, Choi C-G, Kim SJ. Histogram analysis of intravoxel incoherent motion for differentiating recurrent tumor from treatment effect in patients with glioblastoma: initial clinical experience. *AJNR Am J Neuroradiol.* (2014) 35:490–7. doi: 10.3174/ajnr.A3719
  68. Patel P, Baradaran H, Delgado D, Askin G, Christos P, John Tsiouris A, et al. MR perfusion-weighted imaging in the evaluation of high-grade gliomas after treatment: a systematic review and meta-analysis. *Neuro Oncol.* (2017) 19:118–27. doi: 10.1093/neuonc/now148
  69. Seeger A, Braun C, Skardelly M, Paulsen F, Schittenhelm J, Ernemann U, et al. Comparison of three different MR perfusion techniques and MR spectroscopy for multiparametric assessment in distinguishing recurrent high-grade gliomas from stable disease. *Acad Radiol.* (2013) 20:1557–65. doi: 10.1016/j.acra.2013.09.003
  70. Sugahara T, Korogi Y, Tomiguchi S, Shigematsu Y, Ikushima I, Kira T, et al. Posttherapeutic intraaxial brain tumor: the value of perfusion-sensitive contrast-enhanced MR imaging for differentiating tumor recurrence from nonneoplastic contrast-enhancing tissue. *AJNR Am J Neuroradiol.* (2000) 21:901–9.
  71. Prager AJ, Martinez N, Beal K, Omuro A, Zhang Z, Young RJ. Diffusion and perfusion MRI to differentiate treatment-related changes including pseudoprogression from recurrent tumors in high-grade gliomas with histopathologic evidence. *AJNR Am J Neuroradiol.* (2015) 36:877–85. doi: 10.3174/ajnr.A4218
  72. Barajas RF Jr, Chang JS, Segal MR, Parsa AT, McDermott MW, Berger MS, et al. Differentiation of recurrent glioblastoma multiforme from radiation necrosis after external beam radiation therapy with dynamic susceptibility-weighted contrast-enhanced perfusion MR imaging. *Radiology.* (2009) 253:486–96. doi: 10.1148/radiol.2532090007
  73. Iv M, Liu X, Lavezo J, Gentles AJ, Ghanem R, Lumms S, et al. Perfusion MRI-based fractional tumor burden differentiates between tumor and treatment effect in recurrent glioblastomas and informs clinical decision-making. *AJNR Am J Neuroradiol.* (2019) 40:1649–57. doi: 10.3174/ajnr.A6211
  74. Boxerman JL, Schmainda KM, Weisskoff RM. Relative cerebral blood volume maps corrected for contrast agent extravasation significantly correlate with glioma tumor grade, whereas uncorrected maps do not. *AJNR Am J Neuroradiol.* (2006) 27:859–67.
  75. Boxerman JL, Prah DE, Paulson ES, Machan JT, Bedekar D, Schmainda KM. The Role of preload and leakage correction in gadolinium-based cerebral blood volume estimation determined by comparison with MION as a criterion standard. *AJNR Am J Neuroradiol.* (2012) 33:1081–7. doi: 10.3174/ajnr.A2934
  76. Schmainda KM, Rand SD, Joseph AM, Lund R, Ward BD, Pathak AP, et al. Characterization of a first-pass gradient-echo spin-echo method to predict brain tumor grade and angiogenesis. *AJNR Am J Neuroradiol.* (2004) 25:1524–32.
  77. Hu LS, Baxter LC, Pinnaduwege DS, Paine TL, Karis JP, Feuerstein BG, et al. Optimized preload leakage-correction methods to improve the diagnostic accuracy of dynamic susceptibility-weighted contrast-enhanced perfusion MR imaging in posttreatment gliomas. *AJNR Am J Neuroradiol.* (2010) 31:40–8. doi: 10.3174/ajnr.A1787
  78. Welker K, Boxerman J, Kalnin A, Kaufmann T, Shiroishi M, Wintermark M, et al. ASFN recommendations for clinical performance of MR dynamic susceptibility contrast perfusion imaging of the brain. *AJNR Am J Neuroradiol.* (2015) 36:E41–51. doi: 10.3174/ajnr.A4341
  79. Semmineh NB, Bell LC, Stokes AM, Hu LS, Boxerman JL, Quarles CC. Optimization of acquisition and analysis methods for clinical dynamic susceptibility contrast MRI using a population-based digital reference object. *AJNR Am J Neuroradiol.* (2018) 39:1981–8. doi: 10.3174/ajnr.A5827
  80. Conte GM, Castellano A, Altabella L, Iadanza A, Cadioli M, Falini A, et al. Reproducibility of dynamic contrast-enhanced MRI and dynamic susceptibility contrast MRI in the study of brain gliomas: a comparison of data obtained using different commercial software. *Radiol Med.* (2017) 122:294–302. doi: 10.1007/s11547-016-0720-8
  81. Hu LS, Kelm Z, Korfiatis P, Dueck AC, Elrod C, Ellingson BM, et al. Impact of software modeling on the accuracy of perfusion MRI in glioma. *AJNR Am J Neuroradiol.* (2015) 36:2242–9. doi: 10.3174/ajnr.A4451

82. Bell LC, Semmineh N, An H, Eldeniz C, Wahl R, Schmainda KM, et al. Evaluating the use of rCBV as a tumor grade and treatment response classifier across NCI quantitative imaging network sites: part II of the DSC-MRI digital reference object (DRO) challenge. *Tomography*. (2020) 6:203–8. doi: 10.18383/j.tom.2020.00012
83. Schmainda KM, Prah MA, Rand SD, Liu Y, Logan B, Muzi M, et al. Multisite concordance of DSC-MRI analysis for brain tumors: results of a national cancer institute quantitative imaging network collaborative project. *AJNR Am J Neuroradiol*. (2018) 39:1008–16. doi: 10.3174/ajnr.A5675
84. Bell LC, Semmineh N, An H, Eldeniz C, Wahl R, Schmainda KM, et al. Evaluating multisite rCBV consistency from DSC-MRI imaging protocols and postprocessing software across the NCI Quantitative Imaging Network sites using a digital reference object (DRO). *Tomography*. (2019) 5:110–7. doi: 10.18383/j.tom.2018.00041
85. Bedekar D, Jensen T, Schmainda KM. Standardization of relative cerebral blood volume (rCBV) image maps for ease of both inter- and inpatient comparisons. *Magn Reson Med*. (2010) 64:907–13. doi: 10.1002/mrm.22445
86. Winkler F, Kozin SV, Tong RT, Chae S-S, Booth MF, Garkavtsev I, et al. Kinetics of vascular normalization by VEGFR2 blockade governs brain tumor response to radiation. *Cancer Cell*. (2004) 6:553–63. doi: 10.1016/j.ccr.2004.10.011
87. Batchelor TT, Sorensen AG, di Tomaso E, Zhang W-T, Duda DG, Cohen KS, et al. AZD2171, a pan-VEGF receptor tyrosine kinase inhibitor, normalizes tumor vasculature and alleviates edema in glioblastoma patients. *Cancer Cell*. (2007) 11:83–95. doi: 10.1016/j.ccr.2006.11.021
88. Schmainda KM, Prah M, Connelly J, Rand SD, Hoffman RG, Mueller W, et al. Dynamic-susceptibility contrast agent MRI measures of relative cerebral blood volume predict response to bevacizumab in recurrent high-grade glioma. *Neuro Oncol*. (2014) 16:880–8. doi: 10.1093/neuonc/not216
89. Cuccarini V, Aquino D, Gioppo A, Anghileri E, Pellegatta S, Schettino C, et al. Advanced MRI assessment during dendritic cell immunotherapy added to standard treatment against glioblastoma. *J Clin Med*. (2019) 8:2007. doi: 10.3390/jcm8112007
90. Qin L, Li X, Stroiney A, Qu J, Helgager J, Reardon DA, et al. Advanced MRI assessment to predict benefit of anti-programmed cell death 1 protein immunotherapy response in patients with recurrent glioblastoma. *Neuroradiology*. (2017) 59:135–45. doi: 10.1007/s00234-016-1769-8
91. Neuwelt EA, Varallyay CG, Manning R, Solyosi D, Haluska M, Hunt MA, et al. The potential of ferumoxytol nanoparticle magnetic resonance imaging, perfusion, and angiography in central nervous system malignancy: a pilot study. *Neurosurgery*. (2007) 60:601–11; discussion 611–2. doi: 10.1227/01.NEU.0000255350.71700.37
92. Gahramanov S, Raslan AM, Muldoon LL, Hamilton BE, Rooney WD, Varallyay CG, et al. Potential for differentiation of pseudoprogression from true tumor progression with dynamic susceptibility-weighted contrast-enhanced magnetic resonance imaging using ferumoxytol vs. gadoteridol: a pilot study *Int J Radiat Oncol Biol Phys*. (2011) 79:514–23. doi: 10.1016/j.ijrobp.2009.10.072
93. Toth GB, Varallyay CG, Horvath A, Bashir MR, Choyke PL, Daldrup-Link HE, et al. Current and potential imaging applications of ferumoxytol for magnetic resonance imaging. *Kidney Int*. (2017) 92:47–66. doi: 10.1016/j.kint.2016.12.037
94. Varallyay CG, Muldoon LL, Gahramanov S, Wu YJ, Goodman JA Li X, et al. Dynamic MRI using iron oxide nanoparticles to assess early vascular effects of antiangiogenic versus corticosteroid treatment in a glioma model. *J Cereb Blood Flow Metab*. (2009) 29:853–60. doi: 10.1038/jcbfm.2008.162
95. McConnell HL, Schwartz DL, Richardson BE, Woltjer RL, Muldoon LL, Neuwelt EA. Ferumoxytol nanoparticle uptake in brain during acute neuroinflammation is cell-specific. *Nanomedicine*. (2016) 12:1535–42. doi: 10.1016/j.nano.2016.03.009
96. Barajas RF, Hamilton BE, Schwartz D, McConnell HL, Pettersson DR, Horvath A, et al. Combined iron oxide nanoparticle ferumoxytol and gadolinium contrast enhanced MRI define glioblastoma pseudoprogression. *Neuro Oncol*. (2019) 21:517–26. doi: 10.1093/neuonc/noy160
97. Vasanawala SS, Nguyen K-L, Hope MD, Bridges MD, Hope TA, Reeder SB, et al. Safety and technique of ferumoxytol administration for MRI: safety and Technique of Ferumoxytol Administration for MRI. *Magn Reson Med*. (2016) 75:2107–11. doi: 10.1002/mrm.26151
98. Bell LC, Hu LS, Stokes AM, McGee SC, Baxter LC, Quarles CC. Characterizing the influence of preload dosing on percent signal recovery (PSR) and cerebral blood volume (CBV) measurements in a patient population with high-grade glioma using dynamic susceptibility contrast MRI. *Tomography*. (2017) 3:89–95. doi: 10.18383/j.tom.2017.00004
99. Morabito R, Alafaci C, Pergolizzi S, Pontoriero A, Iati' G, Bonanno L, et al. DCE and DSC perfusion MRI diagnostic accuracy in the follow-up of primary and metastatic intra-axial brain tumors treated by radiosurgery with cyberknife. *Radiat Oncol*. (2019) 14:65. doi: 10.1186/s13014-019-1271-7
100. Hamilton JD, Lin J, Ison C, Leeds NE, Jackson EF, Fuller GN, et al. Dynamic contrast-enhanced perfusion processing for neuroradiologists: model-dependent analysis may not be necessary for determining recurrent high-grade glioma versus treatment effect. *AJNR Am J Neuroradiol*. (2015) 36:686–93. doi: 10.3174/ajnr.A4190
101. Bisdas S, Naegel T, Ritz R, Dimostheni A, Pfannenber C, Reimold M, et al. Distinguishing recurrent high-grade gliomas from radiation injury: a pilot study using dynamic contrast-enhanced MR imaging. *Acad Radiol*. (2011) 18:575–83. doi: 10.1016/j.acra.2011.01.018
102. Barboriak DP, Zhang Z, Desai P, Snyder BS, Safriel Y, McKinstry RC, et al. Interreader variability of dynamic contrast-enhanced MRI of recurrent glioblastoma: the multicenter ACRIN 6677/RTOG 0625 study. *Radiology*. (2019) 290:467–76. doi: 10.1148/radiol.2019181296
103. Anzalone N, Castellano A, Cadioli M, Conte GM, Cuccarini V, Bizzi A, et al. Brain gliomas: multicenter standardized assessment of dynamic contrast-enhanced and dynamic susceptibility contrast MR images. *Radiology*. (2018) 287:933–43. doi: 10.1148/radiol.2017170362
104. Petcharunpaisan S, Ramalho J, Castillo M. Arterial spin labeling in neuroimaging. *World J Radiol*. (2010) 2:384–98. doi: 10.4329/wjr.v2.i10.384
105. Jovanovic M, Radenkovic S, Stosic-Opincal T, Lavrnica S, Gavrilovic S, Lazovic-Popovic B, et al. Differentiation between progression and pseudoprogression by arterial spin labeling MRI in patients with glioblastoma multiforme. *J BUON*. (2017) 22:1061–7.
106. Nyberg E, Honce J, Kleinschmidt-DeMasters BK, Shukri B, Kreidler S, Nagae L. Arterial spin labeling: pathologically proven superiority over conventional MRI for detection of high-grade glioma progression after treatment. *Neuroradiol J*. (2016) 29:377–83. doi: 10.1177/1971400916665375
107. Ozsunar Y, Mullins ME, Kwong K, Hochberg FH, Ament C, Schaefer PW, et al. Glioma recurrence versus radiation necrosis? A pilot comparison of arterial spin-labeled, dynamic susceptibility contrast enhanced MRI, and FDG-PET imaging. *Acad Radiol*. (2010) 17:282–90. doi: 10.1016/j.acra.2009.10.024
108. Choi YJ, Kim HS, Jahng G-H, Kim SJ, Suh DC. Pseudoprogression in patients with glioblastoma: added value of arterial spin labeling to dynamic susceptibility contrast perfusion MR imaging. *Acta Radiol*. (2013) 54:448–54. doi: 10.1177/0284185112474916
109. Ippolito L, Morandi A, Giannoni E, Chiarugi P. Lactate: a metabolic driver in the tumour landscape. *Trends Biochem Sci*. (2019) 44:153–66. doi: 10.1016/j.tibs.2018.10.011
110. Choi C, Ganji SK, DeBerardinis RJ, Hatanpaa KJ, Rakheja D, Kovacs Z, et al. 2-hydroxyglutarate detection by magnetic resonance spectroscopy in IDH-mutated patients with gliomas. *Nat Med*. (2012) 18:624–9. doi: 10.1038/nm.2682
111. Croteau D, Scarpace L, Hearshen D, Gutierrez J, Fisher JL, Rock JP, et al. Correlation between magnetic resonance spectroscopy imaging and image-guided biopsies: semiquantitative and qualitative histopathological analyses of patients with untreated glioma. *Neurosurgery*. (2001) 49:823–9. doi: 10.1227/00006123-200110000-00008
112. Rock JP, Hearshen D, Scarpace L, Croteau D, Gutierrez J, Fisher JL, et al. Correlations between magnetic resonance spectroscopy and image-guided histopathology, with special attention to radiation necrosis. *Neurosurgery*. (2002) 51:912–9; discussion 919–20. doi: 10.1097/00006123-200210000-00010
113. Rock JP, Scarpace L, Hearshen D, Gutierrez J, Fisher JL, Rosenblum M, et al. Associations among magnetic resonance spectroscopy, apparent diffusion coefficients, and image-guided histopathology with special attention to radiation necrosis. *Neurosurgery*. (2004) 54:1111–7; discussion 1117–9. doi: 10.1227/01.neu.0000119328.56431.a7

114. Fink JR, Carr RB, Matsusue E, Iyer RS, Rockhill JK, Haynor DR, et al. Comparison of 3 Tesla proton MR spectroscopy, MR perfusion and MR diffusion for distinguishing glioma recurrence from posttreatment effects. *J Magn Reson Imaging*. (2012) 35:56–63. doi: 10.1002/jmri.22801
115. Hu LS, Wang L, Hawkins-Daarud A, Eschbacher JM, Singleton KW, Jackson PR, et al. Uncertainty quantification in the radiogenomics modeling of EGFR amplification in glioblastoma. *Sci Rep*. (2021) 11:3932. doi: 10.1038/s41598-021-83141-z
116. Hu LS, Ning S, Eschbacher JM, Baxter LC, Gaw N, Ranjbar S, et al. Radiogenomics to characterize regional genetic heterogeneity in glioblastoma. *Neuro Oncol*. (2017) 19:128–37. doi: 10.1093/neuonc/now135
117. Hu LS, Ning S, Eschbacher JM, Gaw N, Dueck AC, Smith KA, et al. Multi-parametric MRI and texture analysis to visualize spatial histologic heterogeneity and tumor extent in Glioblastoma. *PLoS One*. (2015) 10:e0141506. doi: 10.1371/journal.pone.0141506
118. Akbari H, Rathore S, Bakas S, Nasrallah MP, Shukla G, Mamourian E, et al. Histopathology-validated machine learning radiographic biomarker for noninvasive discrimination between true progression and pseudo-progression in glioblastoma. *Cancer*. (2020) 126:2625–36. doi: 10.1002/cncr.32790
119. Gao Y, Xiao X, Han B, Li G, Ning X, Wang D, et al. Deep learning methodology for differentiating glioma recurrence from radiation necrosis using multimodal magnetic resonance imaging: algorithm development and validation (preprint). *JMIR Preprints*. (2020). doi: 10.2196/preprints.19805
120. Zach L, Guez D, Last D, Daniels D, Grober Y, Nissim O, et al. Delayed contrast extravasation MRI: a new paradigm in neuro-oncology. *Neuro Oncol*. (2015) 17:457–65. doi: 10.1093/neuonc/nou230

**Conflict of Interest:** KSw was co-founder of Precision Oncology Insights, US Patent US8571844B2. KSc: financial interest—Imaging Biometrics LLC; ownership interest—IQ-AQ Ltd; ownership interest—Prism Clinical Imaging, Inc. LH: Imaging Biometrics (Medical Advisory Board); Precision Oncology Insights (co-founder), Bayer Pharmaceutical (paid speaker), US Patent Number 10,909,675.

The remaining authors declare that the research was conducted in the absence of any commercial or financial relationships that could be construed as a potential conflict of interest.

**Publisher's Note:** All claims expressed in this article are solely those of the authors and do not necessarily represent those of their affiliated organizations, or those of the publisher, the editors and the reviewers. Any product that may be evaluated in this article, or claim that may be made by its manufacturer, is not guaranteed or endorsed by the publisher.

Copyright © 2022 Malik, Rath, Urcuyo Acevedo, Canoll, Swanson, Boxerman, Quarles, Schmainda, Burns and Hu. This is an open-access article distributed under the terms of the Creative Commons Attribution License (CC BY). The use, distribution or reproduction in other forums is permitted, provided the original author(s) and the copyright owner(s) are credited and that the original publication in this journal is cited, in accordance with accepted academic practice. No use, distribution or reproduction is permitted which does not comply with these terms.